Supporting Information

Rational design of phenanthroimidazole-diarylsulfone derivatives as efficient blue hot exciton emitters with hybridized local and charge transfer state

Suangsiri Arunlimsawat[a], Teerapat Itsoponpan[a], Phattananawee Nalaoh[a], Taweesak Sudyoadsuk[b] and Vinich Promarak[a]*

[a] Department of Materials Science and Engineering, School of Molecular Science and Engineering, Vidyasirimedhi Institute of Science and Technology, Wangchan, Rayong 21210, Thailand,
[b] Frontier Research Center (FRC), Vidyasirimedhi Institute of Science and Technology, Wangchan, Rayong 21210, Thailand
E-mail: vinich.p@vistec.ac.th

Synthesis and characterization

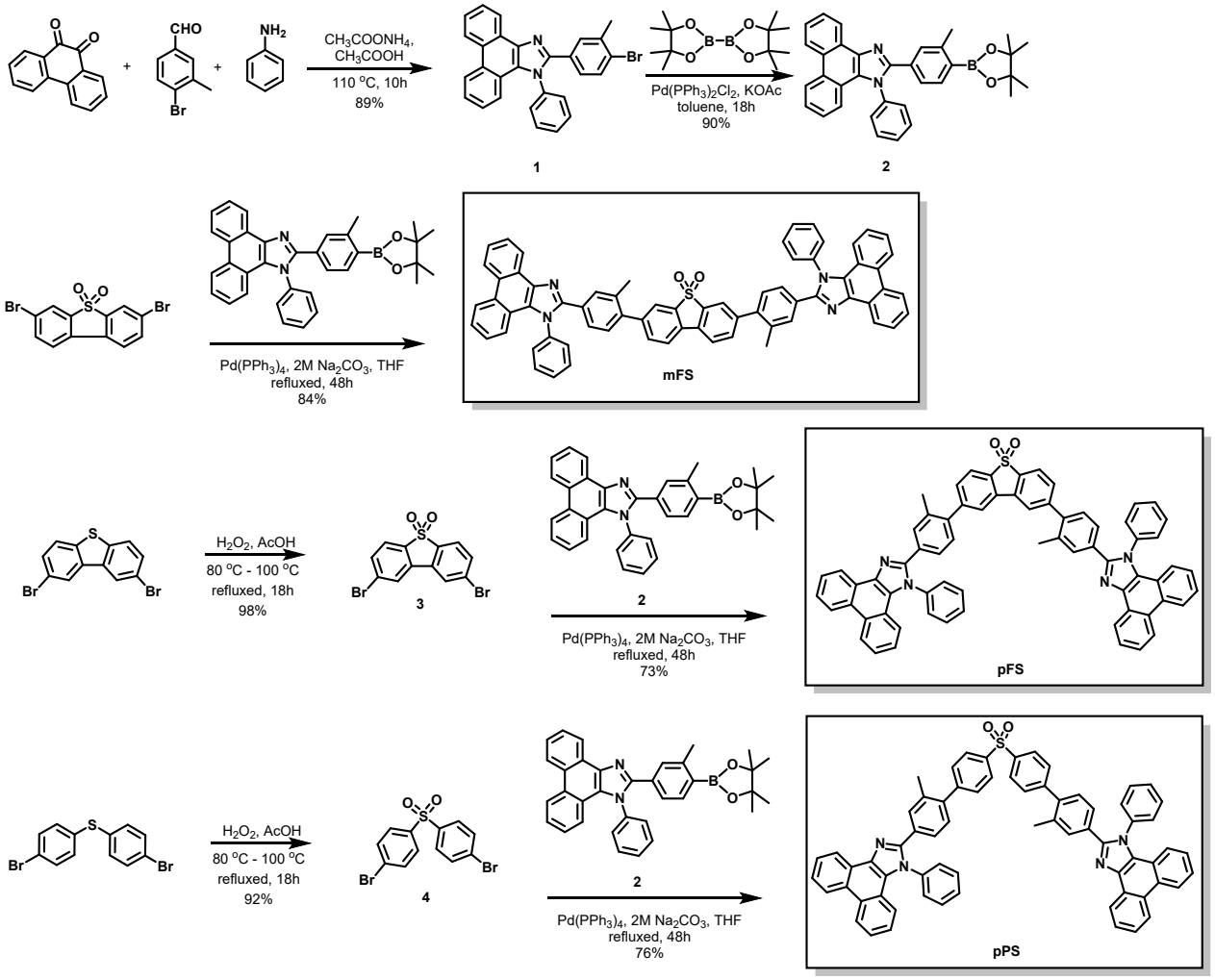

Scheme S1: Synthetic route of **mFS**, **pFS,** and **pPS.**

Synthesis of 2-(4-bromo-3-methylphenyl)-1-phenyl-1*H*-phenanthro[9,10-*d*]imidazole (1): Phenanthrenequinone (2.00 g, 9.606 mmol) and 4-bromo-3-methylbenzaldehyde (1.28mL, 9.606 mmol) were placed in a round-bottom flask, and glacial acetic acid was poured into the flask. Then, the mixture was stirred. Aniline (1.32 mL, 14.410 mmol) was added dropwise into the mixture, then ammonium acetate (3.70 g, 48.028 mmol) was added in one portion. The reaction mixture was refluxed at 110 °C as well as kept stirring for 10 h. After that, the color reaction was changed from orange to brown. To stop the reaction, the mixture was cooled down to room temperature, then it was poured into ethanol solution ($EtOH/H_2O$ 4:1, 500 mL). Cream precipitate was filtered and washed several times with the ethanol solution ($EtOH/H_2O$ 4:1) to get rid the rest of glacial acetic acid and other residues from the mixture, then obtain **1** as cream needle-like powder (3.97 g, 89%). ^{1}H NMR (600 MHz, $CDCl_3$) δ 8.86 (d, *J* = 7.9 Hz, 1H), 8.77 (d, *J* = 8.4 Hz, 1H), 8.71 (d, *J* = 8.3 Hz, 1H), 7.74 (t, *J* = 7.3 Hz, 1H), 7.69 – 7.56 (m, 5H), 7.52 (td, *J* = 6.8, 1.6 Hz, 3H), 7.39 (d, *J* = 8.3 Hz, 1H), 7.28 – 7.24 (m, 1H), 7.19 (d, *J* = 8.3 Hz, 1H), 7.08 (dd, *J* = 8.4, 2.3 Hz, 1H), 2.35 (s, 3H). ^{13}C NMR (151 MHz, $CDCl_3$) δ 150.08, 138.79, 138.21, 137.56, 132.19, 132.00, 130.38, 130.07, 129.78, 129.47, 129.20, 128.44, 128.37, 127.87, 127.48, 127.28, 126.45, 126.01, 125.84, 125.13, 124.28, 123.28, 123.11, 122.85, 120.99, 23.05; HMRS–MALDI–TOF (m/z): $[M+H]^+$ calcd for $C_{28}H_{19}BrN_2$, 463.0804; found, 463.0804.

Synthesis of 2-(3-methyl-4-(4,4,5,5-tetramethyl-1,3,2-dioxaborolan-2-yl)phenyl)-1-phenyl-1*H*-phenanthro[9,10-*d*]imidazole (2): A mixture of **1** (723 mg, 1.561 mmol), bis(pinacolato)diboron (1.19 g, 4.684 mmol), KOAc (1.84g, 18.734 mmol) and $Pd(dppf)Cl_2$ (82.2 mg, 0.117 mmol) in dry toluene (40 mL) was degassed with N_2 for 10 min. The reaction mixture was stirred at a refluxing temperature under N_2 atmosphere for 18 h. After being cooled to room temperature, the mixture was diluted with water (100 mL) and extracted with CH_2Cl_2 (50 mL x 3). The combined organic layer was washed with water, brine, dried over anhydrous Na_2SO_4, filtered, and concentrated under reduced pressure. The crude product was purified by column chromatography over silica gel eluting with CH_2Cl_2/hexane 4:1 to get rid all impurities, then eluting with pure CH_2Cl_2 to obtain **2** as white solid (715.4 mg, 90%). ^{1}H NMR (600 MHz, $CDCl_3$) δ 8.89 (d, *J* = 8.1 Hz, 1H), 8.77 (d, *J* = 8.3 Hz, 1H), 8.70 (d, *J* = 8.3 Hz, 1H), 7.74 (t, *J* = 7.4 Hz, 1H), 7.68 – 7.56 (m, 6H), 7.53 – 7.47 (m, 3H), 7.28-7.23 (m, 1H), 7.18 (dd, *J* = 7.6, 3.9 Hz, 2H), 2.50 (s, 3H), 1.34 (s, 12H). ^{13}C NMR (151 MHz, $CDCl_3$) δ 151.02, 144.97, 138.97, 137.62, 135.61, 132.52, 130.97, 130.22, 129.85, 129.43, 129.26, 128.39, 128.36, 127.39, 127.38, 126.37, 125.72, 125.34, 124.99, 124.23, 123.22, 123.20, 122.96, 121.04, 83.71, 25.05, 22.31; HMRS–MALDI–TOF (m/z): $[M]^+$ calcd for $C_{34}H_{31}BN_2O_2$, 510.2479; found, 510.2478.

Synthesis of 2,8-dibromodibenzo[*b,d*]thiophene 5,5-dioxide (3): A round-bottomed flask containing 2,8-dibromodibenzo[b,d]thiophene (400.0 mg, 1.169 mmol) in glacial acetic acid (24 mL) had been stirring for 30 min together with heating at 80°C to get homogeneous solution. Hydrogen peroxide 30% solution (10 mL) was added slowly in the flask, then the mixture was heated to 100 °C as well as kept stirring for 18 h. After being cooled to room temperature, precipitate was formed, filtered and washed with ethanol solution ($EtOH/H_2O$ 4:1), then dried overnight at 700 °C to obtain compound **3** as white solid (428.8 mg, 98%). ^{1}H NMR (600 MHz, $CDCl_3$) δ 7.93 (s, 2H), 7.70 (s, 4H). ^{13}C NMR (151 MHz, $CDCl_3$) δ 136.97, 134.15, 132.38, 128.99, 125.33, 123.81; HMRS– APCI–TOF (m/z): $[M]^+$ calcd for $C_{12}H_6Br_2O_2S$, 372.8528; found, 372.8541.

Synthesis of 4,4'-sulfonylbis(bromobenzene) (4): A round-bottomed flask containing bis(4-bromophenyl) sulfide (460.0 mg, 1.163 mmol) in glacial acetic acid (12 mL) had been stirring for 30 min together with heating at 80°C to get homogeneous solution. Hydrogen peroxide 30% solution (5.88 mL) was added slowly in the flask, then the mixture was heated to 100 °C as well as kept stirring for 18 h. After being cooled to room temperature, the mixture was poured into water, then extracted with CH_2Cl_2 (50 mL x 3). The combined organic layer was washed with water, brine, dried over anhydrous Na_2SO_4, filtered, and concentrated under reduced pressure. The crude product was then purified by column chromatography over silica gel eluting with

CH_2Cl_2/hexane 2:3 to give compound **4** as white solid (401.3 mg, 92%). ^{1}H NMR (600 MHz, $CDCl_3$) δ 7.78 (d, *J* = 8.3 Hz, 4H), 7.65 (d, *J* = 8.4 Hz, 4H). ^{13}C NMR (151 MHz, $CDCl_3$) δ 140.36, 132.91, 129.32, 128.96; HMRS–APCI–TOF (m/z): $[M+H]^+$ calcd for $C_{12}H_8Br_2O_2S$, 374.8685; found, 374.8689.

SCXRD data and refinement

The crystallographic information (CIF) data as depositing with the CCDC number of 2044143, 2044144, and 2047432 for ***m*FS**, ***p*FS**, and ***p*PS**, respectively, were deposited on and can be obtained with no cost at https://www.ccdc.cam.ac.uk/.

Table S1. Crystallographic data of ***m*FS**, ***p*FS**, and ***p*PS**

Compound name	***m*FS**	***p*FS**	***p*PS**
CCDC deposition number	2044143	2044144	2047432
Empirical formula	$C_{70}H_{46}Cl_6N_4O_2S$	$C_{68}H_{44}N_4O_2S$	$C_{68}H_{46}N_4O_2S$
Formula weight	1219.87	981.13	983.15
Temperature/K	100	100	100
Crystal system	triclinic	monoclinic	triclinic
Space group	*P–1*	*C*2/*c*	*P–1*
a/Å b/Å c/Å	12.2956(3) 15.2452(4) 18.7911(5)	15.6108(14) 12.5335(10) 27.274(3)	10.8683(8) 17.8339(13) 28.827(2)
α/° β/° γ/°	96.787(2) 109.019(2) 107.0090(10)	90 97.609(3) 90	90.706(3) 100.716(3) 95.371(3)
Volume/Å^3	3094.34(14)	5289.5(8)	5463.3(7)
Z	2	4	4
ρ_{calc}g/cm^3	1.309	1.232	1.195
μ/mm^{-1}	3.234	0.112	0.109
F(000)	1256.0	2048.0	2056.0
Crystal size/mm^3	0.580 × 0.155 × 0.038	0.65 × 0.40 × 0.25	0.669 × 0.121 × 0.107
Radiation	CuKα (λ = 1.54178)	MoKα (λ = 0.71073)	MoKα (λ = 0.71073)
2Θ range for data collection/°	6.238 to 133.192	4.182 to 54.202	3.734 to 50.054
Index ranges	-14 ≤ h ≤ 14 -18 ≤ k ≤ 18 -21 ≤ l ≤ 22	-20 ≤ h ≤ 20 -16 ≤ k ≤ 16 -34 ≤ l ≤ 34	-12 ≤ h ≤ 12 -21 ≤ k ≤ 21 -34 ≤ l ≤ 34
Reflections collected	38677	71873	109180
Independent reflections	10950 [R_{int} = 0.0684, R_{sigma} = 0.0574]	5833 [R_{int} = 0.0477, R_{sigma} = 0.0247]	19260 [R_{int} = 0.0986, R_{sigma} = 0.0617]
Data/restraints/parameters	10950/0/804	5833/0/340	19260/0/1365
Goodness-of-fit on F^2	1.040	1.029	1.026
Final R indexes [I>=2σ (I)]	R_1 = 0.0528, wR_2 = 0.1246	R_1 = 0.0463, wR_2 = 0.1127	R_1 = 0.0544, wR_2 = 0.1192
Final R indexes [all data]	R_1 = 0.0892, wR_2 = 0.1330	R_1 = 0.0559, wR_2 = 0.1188	R_1 = 0.0892, wR_2 = 0.1330
Largest diff. peak/hole / e Å^{-3}	0.27/-0.41	0.44/-0.47	0.27/-0.41

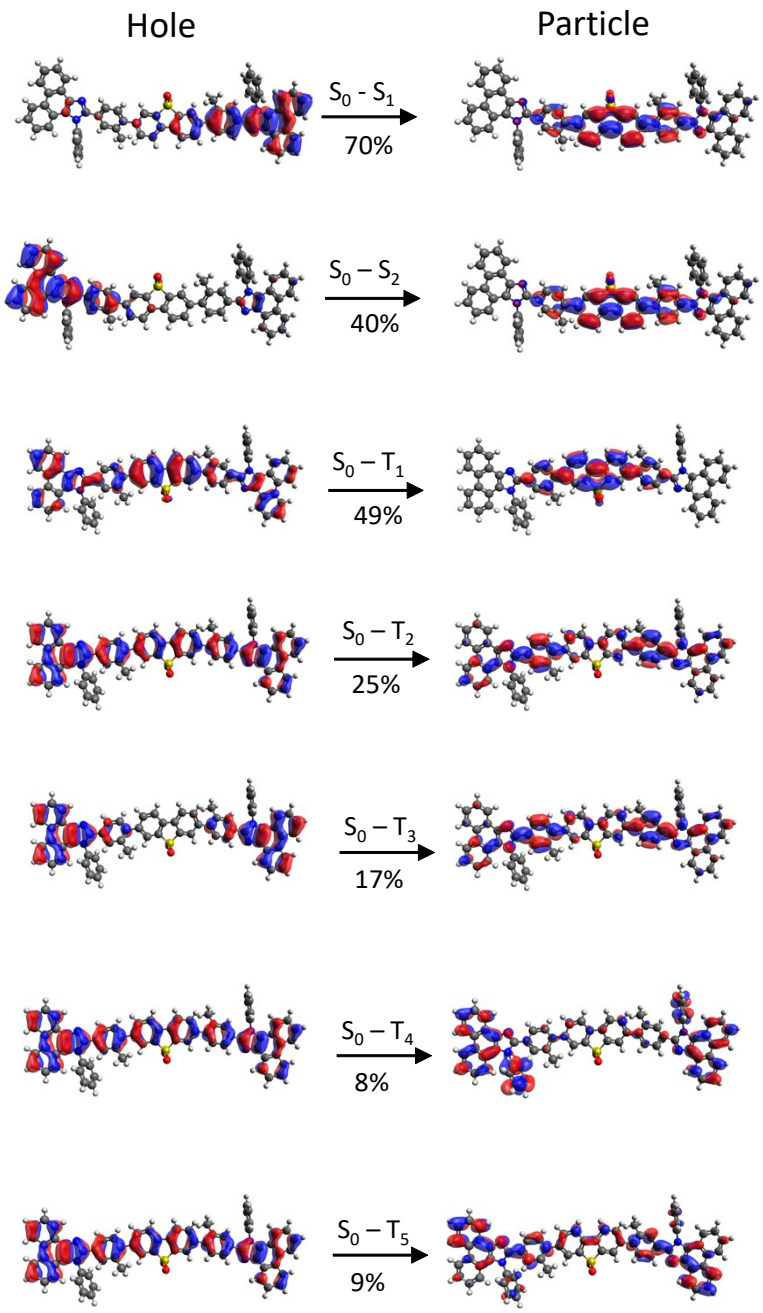

Figure S1 NTOs of ***m*FS** calculated by TD-CAM-B3LYP/6-31G(d,p).

Table S2 Excited states energies of ***m*FS** calculated by TD-CAM-B3LYP/6-31G(d,p).

State	Energy (eV)	Osc. Strength	Transition character	S_m index
S1	3.16	2.6964	LE+CT	0.47879
S2	3.78	0.1876	LE+CT	0.37795
T1	1.65	-	LE+CT	0.48722
T2	2.58	-	LE+CT	0.32209
T3	2.66	-	LE+CT	0.36035
T4	2.87	-	LE+CT	0.34764
T5	3.04	-	LE+CT	0.34053

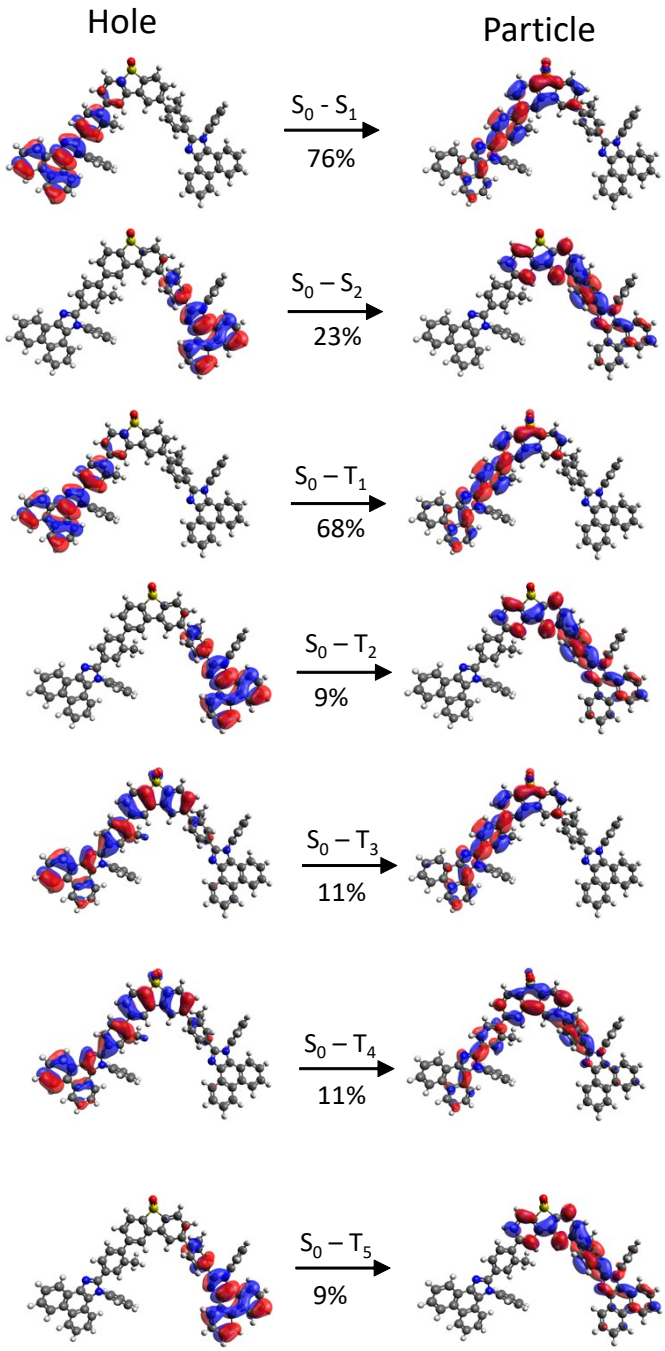

Figure S2 NTOs of ***p*FS** calculated by TD-CAM-B3LYP/6-31G(d,p).

Table S3 Excited states energies of ***p*FS** calculated by TD-CAM-B3LYP/6-31G(d,p).

State	Energy (eV)	Osc. Strength	Transition character	S_m index
S1	3.31	1.5014	LE+CT	0.42031
S2	4.12	0.6563	LE+CT	0.32512
T1	1.59	-	LE+CT	0.50962
T2	2.66	-	LE+CT	0.34303
T3	2.70	-	LE+CT	0.34599
T4	2.87	-	LE+CT	0.34047
T5	3.10	-	LE+CT	0.29479

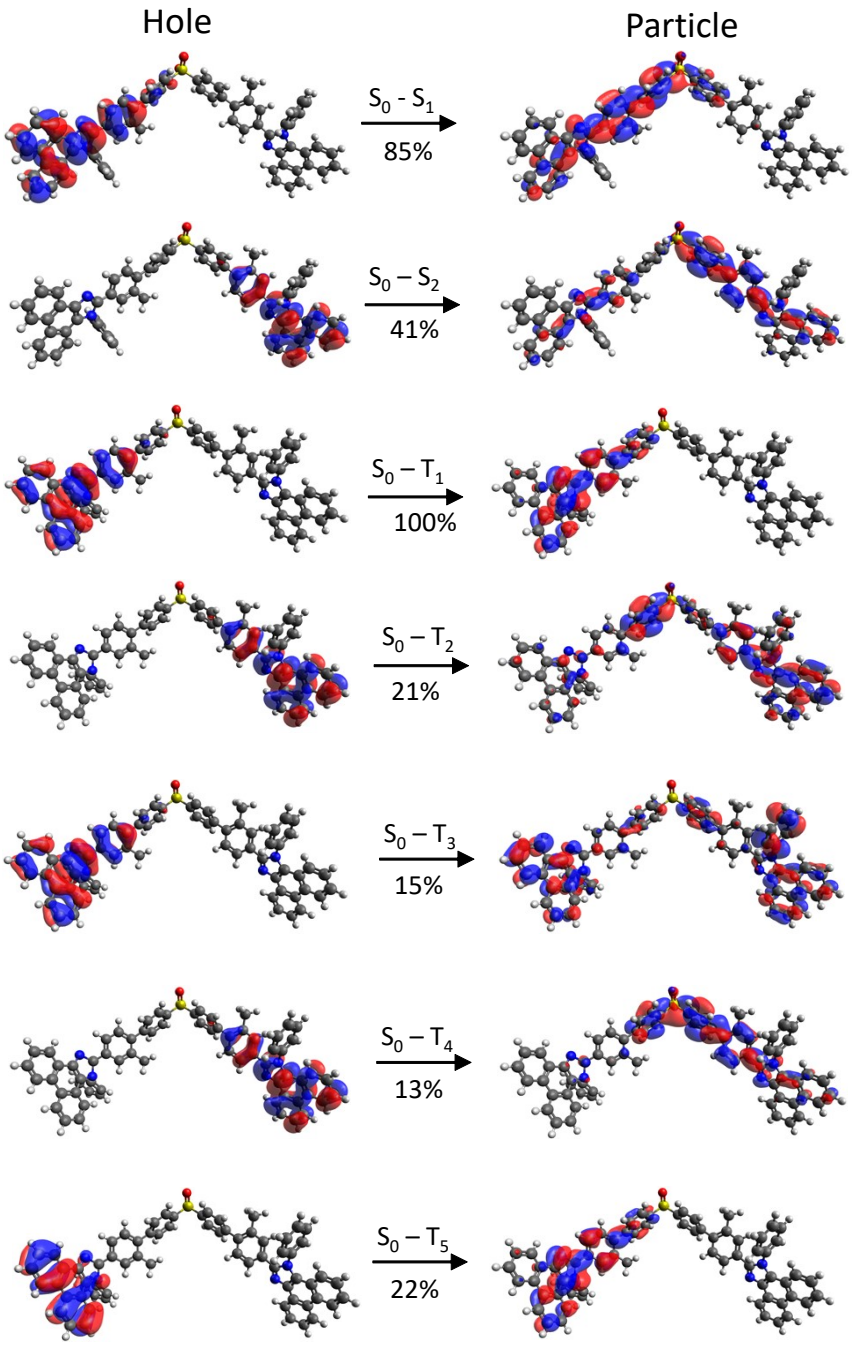

Figure S3 NTOs of ***p*PS** calculated by TD-CAM-B3LYP/6-31G(d,p).

Table S4 Excited states energies of ***p*PS** calculated by TD-CAM-B3LYP/6-31G(d,p).

State	Energy (eV)	Osc. Strength	Transition character	S_m index
S1	3.32	1.6832	LE+CT	0.47190
S2	4.11	0.7544	LE+CT	0.29846
T1	0.77	-	LE+CT	0.50168
T2	2.67	-	LE+CT	0.48356
T3	2.72	-	LE+CT	0.49288
T4	3.05	-	LE+CT	0.34927
T5	3.10	-	LE+CT	0.31871

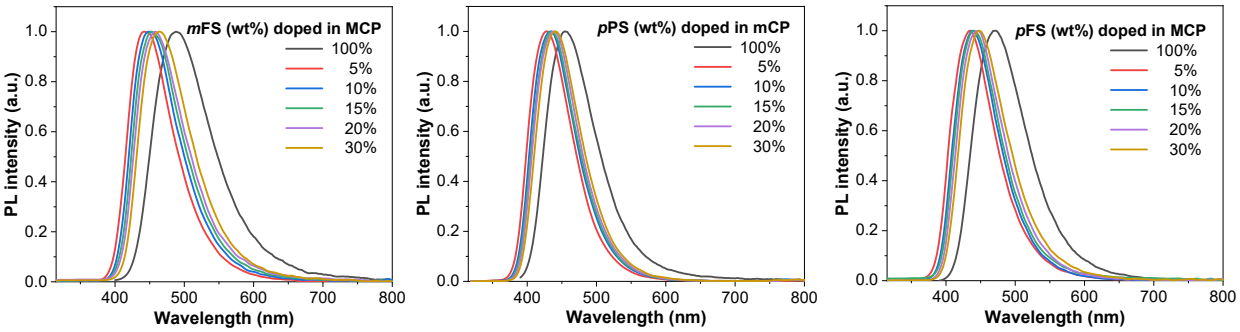

% doped in mCP	*m*FS		*p*PS		*p*FS	
	λ_{Em}(nm)	Φ (%)	λ_{Em}(nm)	Φ (%)	λ_{Em}(nm)	Φ (%)
100% (non-doped film)	**484**	**47**	**448**	**61**	**476**	**31**
5%	442	69	428	95	435	66
10%	**449**	**79**	**433**	**99**	**439**	**77**
15%	453	67	435	90	440	73
20%	458	56	439	92	446	61
30%	464	54	441	90	448	51

Figure S4 PL spectra of the doped thin films and their Φ_{PL} values.

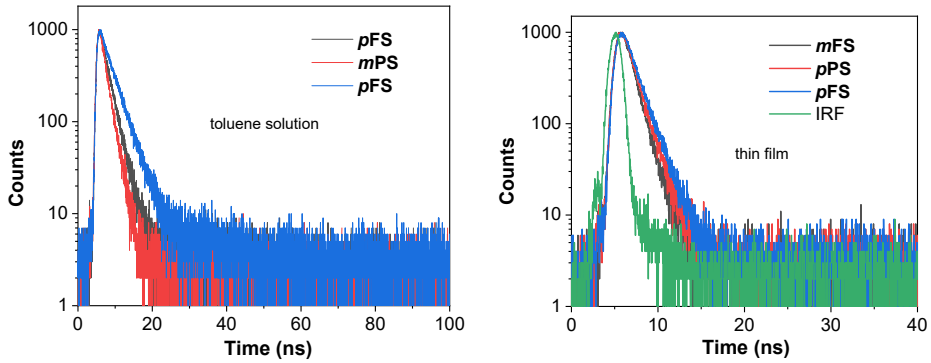

Figure S5 Transient PL decay spectra.

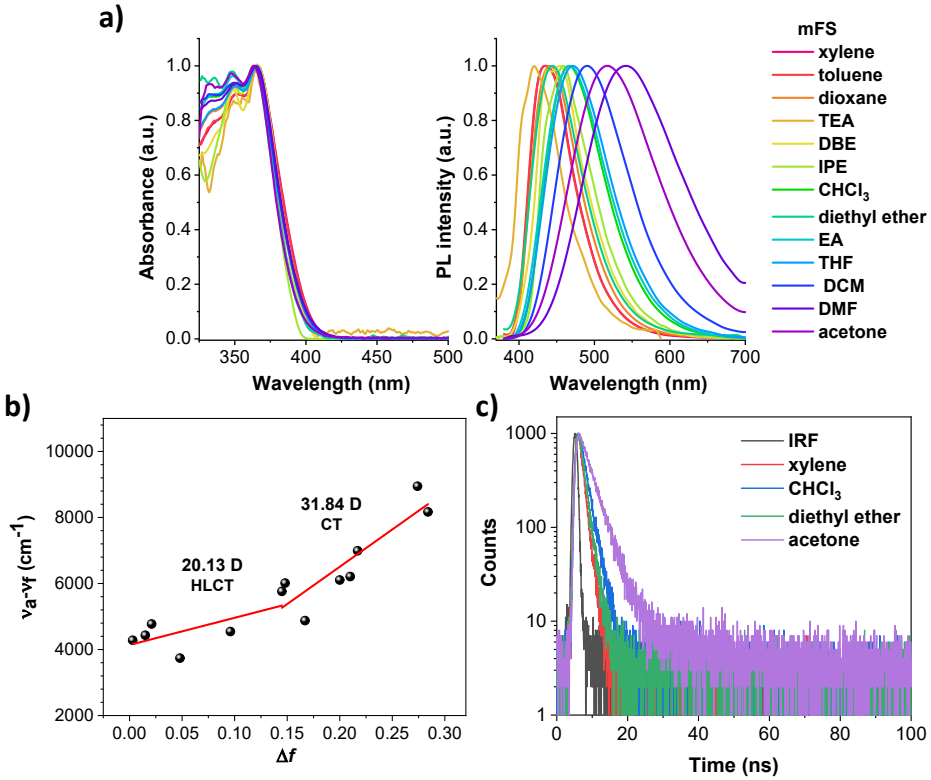

Figure S6 a) UV-vis absorption and PL spectra of ***m*FS** in various solvents. b) Plots of stokes shift (ν_a-ν_f) as a function of the solvent orientation polarizability (Δf)) according to the Lippert Mataga model of ***m*FS**. c) Transient PL decay spectra of ***m*FS** in different solvents.

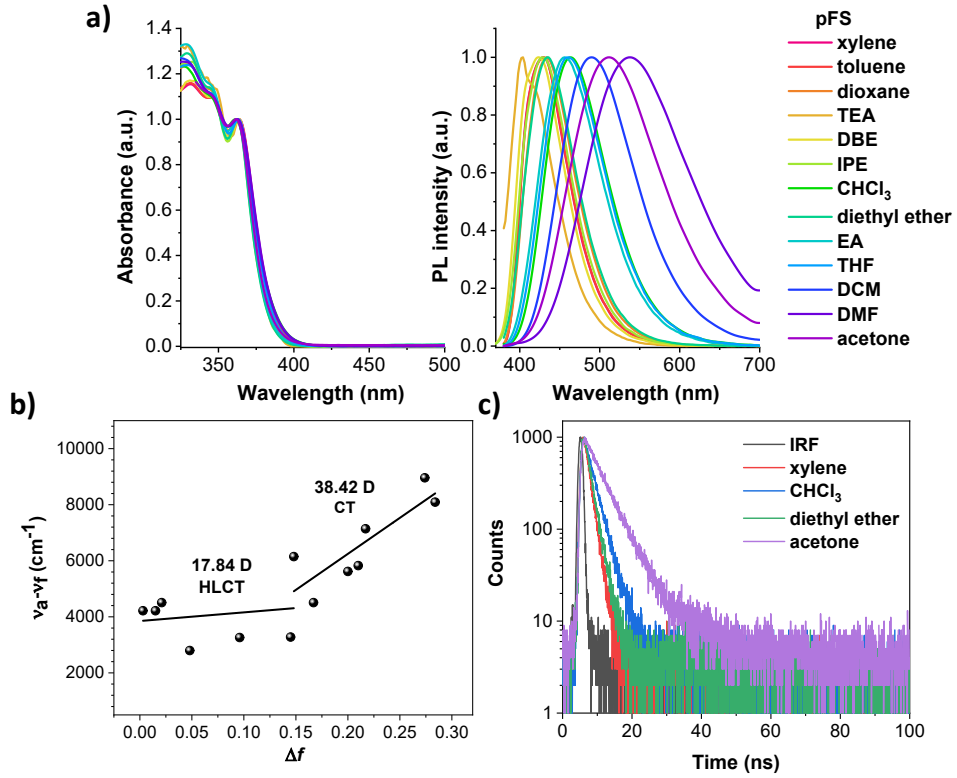

Figure S7 a) UV-vis absorption and PL spectra of ***p*FS** in various solvents. b) Plots of stokes shift (ν_a-ν_f) as a function of the solvent orientation polarizability (Δf)) according to the Lippert Mataga model of ***p*FS**. c) Transient PL decay spectra of ***p*FS** in different solvents.

Lippert–Mataga equation:[1,2]

$$hc(v_a - v_f) = hc\left(v_a^0 - a_f^0\right) + \frac{2(\mu_e - \mu_g)^2}{a_0^3} f(\varepsilon,n)$$

where v_a and v_f are wavenumber of absorption and emission peak, h is a Planck's constant, c is a speed of light, μ_e is the excited-state dipole moment, μ_g is the ground- state dipole moment which can be estimated by DFT calculation, f and a_0 are orientation polarizability and solvent cavity radius, respectively in which can be calculated by following equation.

$$f(\varepsilon,n) = \frac{\varepsilon - 1}{2\varepsilon + 1} + \frac{n^2 - 1}{2n^2 + 1}$$

where ε and n are dielectric constant and refractive index of solvent, respectively

$$a_0 = \frac{3M}{4N\pi d}^{1/3}$$

where N is Avogadro number, M is molecular weight, and d is density (1.0 g cm^{-3})

Table S5 Details of optical data of **mFS, pFS** and **pPS** in different solvents.

				***m*FS**		
Solvent	ε	n	f(ε,n)	λ_a (nm)	λ_f (nm)	ν_a- ν_f (cm^{-1})
Xylene	2.57	1.496	0.003	366	434	4280.93
Toluene	2.38	1.497	0.013	364	434	4431.05
Dioxane	2.22	1.422	0.021	365	442	4772.83
Triethylamine	2.42	1.401	0.048	363	420	3738.69
Dibutyl ether	3.08	1.376	0.096	366	439	4543.36
Isopropyl ether	3.88	1.368	0.145	363	459	5761.72
Chloroform	4.81	1.446	0.148	364	466	6013.30
Diethyl Ether	4.33	1.352	0.167	365	444	4874.74
Ethyl Acetate	6.02	1.372	0.200	364	468	6105.01
Tetrahydrofuran	7.58	1.407	0.210	365	472	6210.82
Dichloromethane	8.93	1.424	0.217	365	490	6989.10
Dimethylformamide	36.7	1.431	0.274	365	542	8947.08
Acetone	20.7	1.359	0.284	363	516	8168.36
				***p*FS**		
Solvent	ε	n	f(ε,n)	λ_a (nm)	λ_f (nm)	ν_a- ν_f (cm^{-1})
Xylene	2.57	1.496	0.003	364	430	4216.71
Toluene	2.38	1.497	0.013	364	430	4216.71
Dioxane	2.22	1.422	0.021	363	434	4506.73
Triethylamine	2.42	1.401	0.048	363	404	2795.73
Dibutyl ether	3.08	1.376	0.096	364	423	3259.45
Isopropyl ether	3.88	1.368	0.145	363	429	3276.36
Chloroform	4.81	1.446	0.148	361	464	6149.11
Diethyl Ether	4.33	1.352	0.167	363	434	4506.73
Ethyl Acetate	6.02	1.372	0.200	363	456	5618.38
Tetrahydrofuran	7.58	1.407	0.210	364	462	5827.51
Dichloromethane	8.93	1.424	0.217	363	490	7140.05

Dimethylformamide	36.7	1.431	0.274	363	538	8960.85
Acetone	20.7	1.359	0.284	362	512	8093.06

Solvent	ε	n	f(ε,n)	***p*PS**		
				λ_a (nm)	λ_f (nm)	ν_a- ν_f (cm^{-1})
Xylene	2.57	1.496	0.003	364	422	3775.85
Toluene	2.38	1.497	0.013	364	422	3775.85
Dioxane	2.22	1.422	0.021	363	424	3963.30
Triethylamine	2.42	1.401	0.048	363	398	2422.58
Dibutyl ether	3.08	1.376	0.096	364	413	3259.45
Isopropyl ether	3.88	1.368	0.145	363	412	3276.36
Chloroform	4.81	1.446	0.148	361	438	4869.78
Diethyl Ether	4.33	1.352	0.167	363	424	3963.30
Ethyl Acetate	6.02	1.372	0.200	363	438	4717.16
Tetrahydrofuran	7.58	1.407	0.210	364	440	4745.25
Dichloromethane	8.93	1.424	0.217	363	450	5325.99
Dimethylformamide	36.7	1.431	0.274	363	474	6451.16
Acetone	20.7	1.359	0.284	362	458	5790.25

ε, n and f(ε,n) are a dielectric constant, a refractive index and an orientation polarization (the Lippert-Mataga function) of solvents, respectively. [2–4]

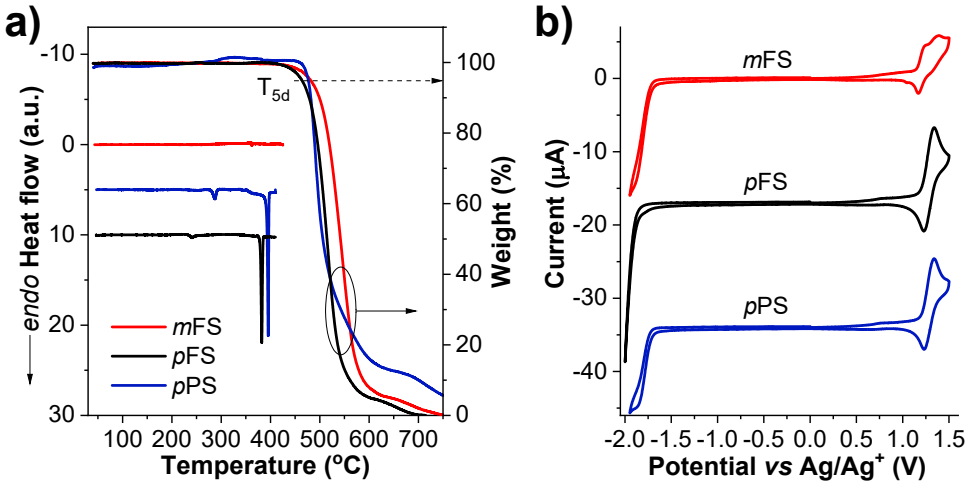

Figure S8 a) TGA and DSC thermograms measured at a heating rate of 10 °C min^{-1} under N_2 flow. b) CV voltammograms analyzed in CH_2Cl_2/*n*-Bu_4NPF_6 at a scan rate of 50 mV s^{-1} under argon atmosphere.

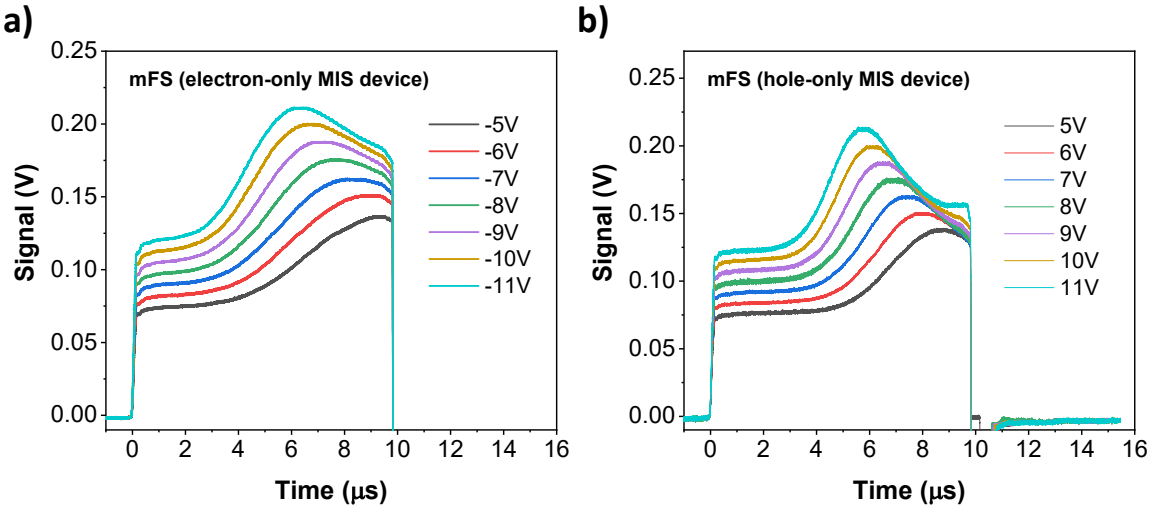

Figure S9 Transient signals of ***m*FS** based MIS devices at different applied maximum voltages for a) electron-only MIS device and b) hole-only MIS device.

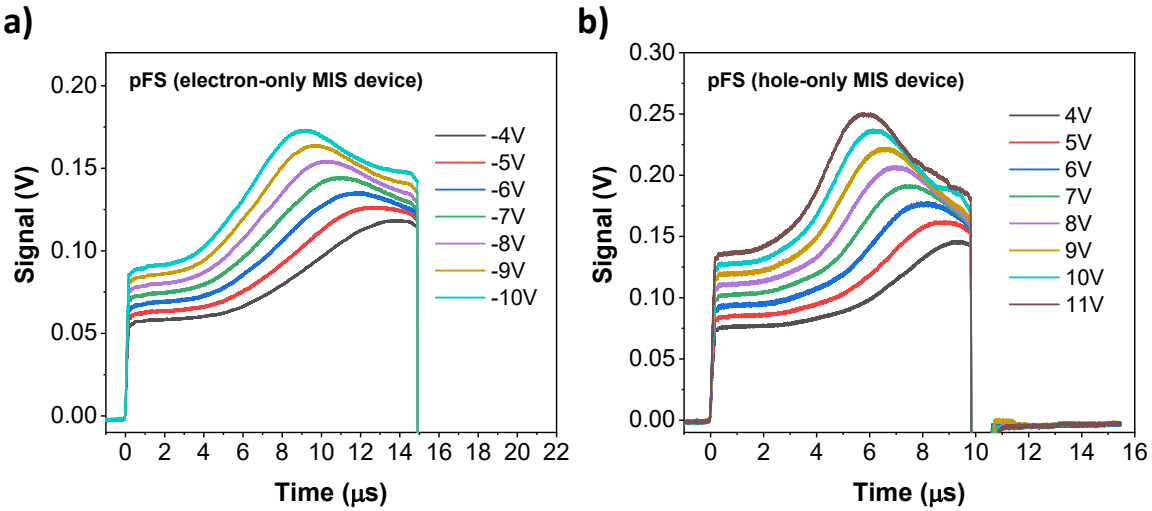

Figure S10 Transient signals of ***p*FS** based MIS devices at different applied maximum voltages for a) electron-only MIS device and b) hole-only MIS device.

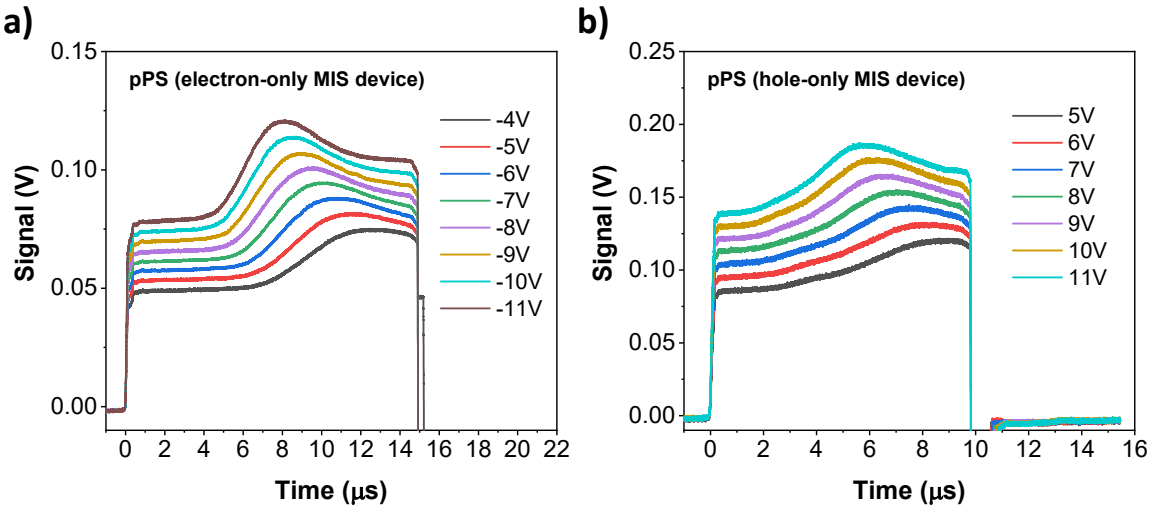

Figure S11 Transient signals of ***p*PS** based MIS devices at different applied maximum voltages for a) electron-only MIS device and b) hole-only MIS device.

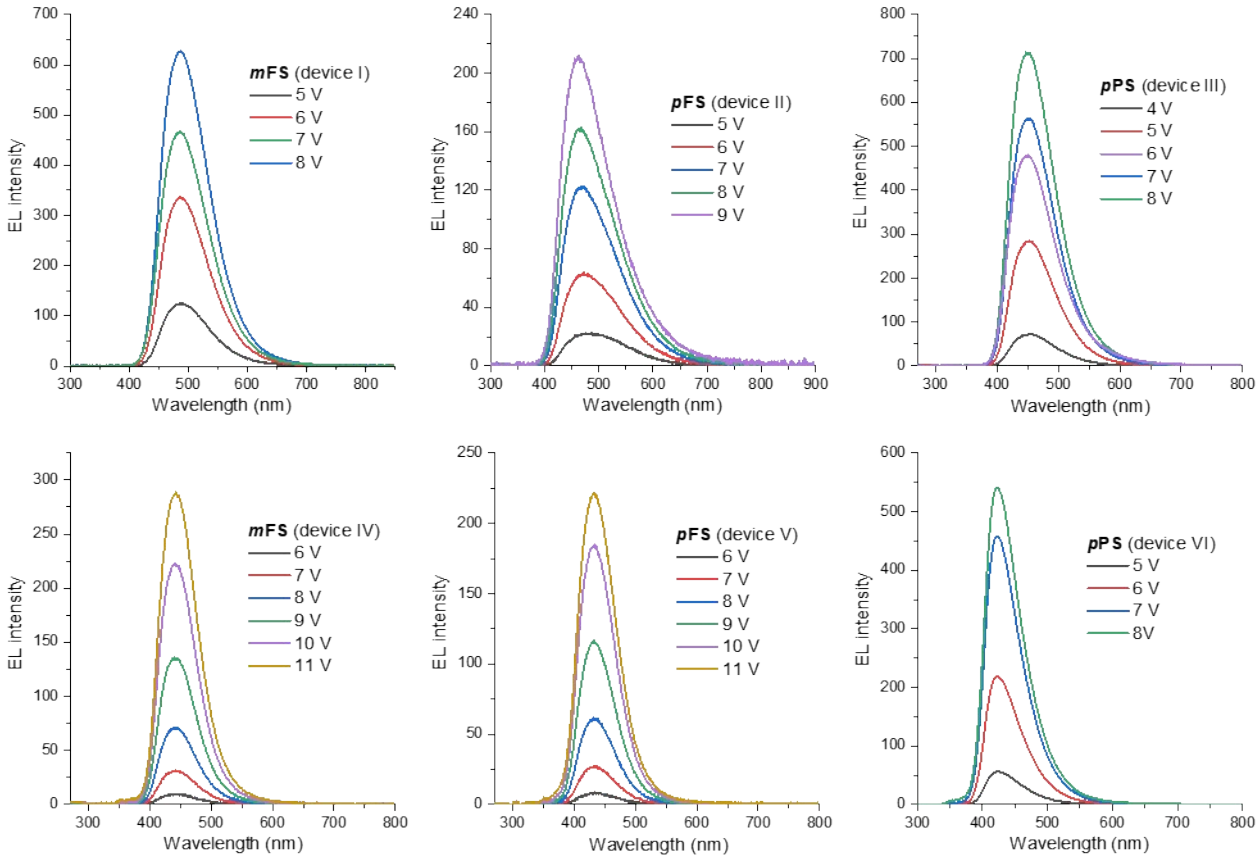

Figure S12 EL spectra of the OLEDs under different applied voltages.

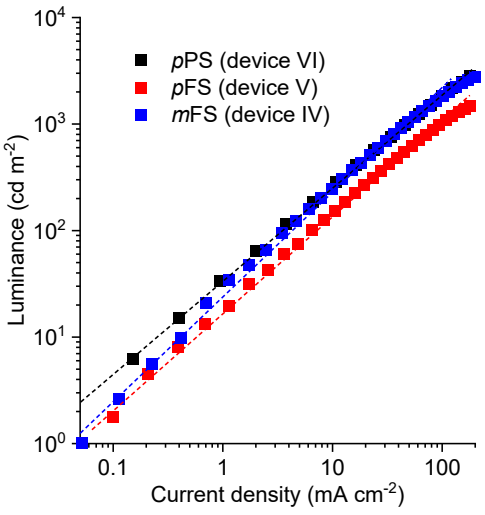

Figure S14 Plots of luminance *vs* current density in a log-log scale of the doped OLEDs (device IV-VI)

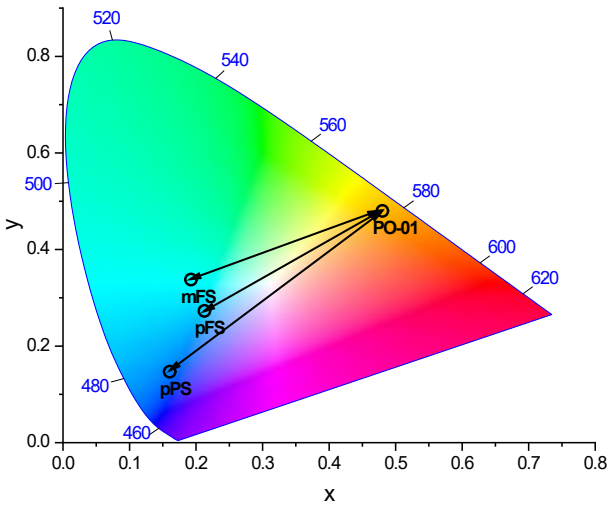

Figure S14 CIE 1931 diagram showing CIExy coordination of ***m*FS**, ***p*FS**, ***p*PS**, and PO-01.

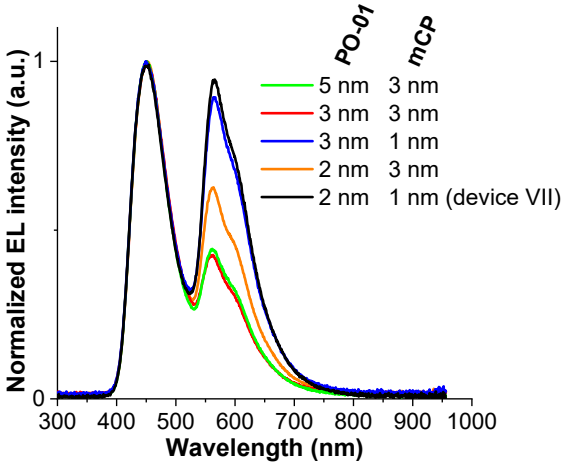

Figure S15 EL spectra of the white OLEDs with different thicknesses of the thin layers of PO-01 (2-5 nm) and mCP (1-3 nm).

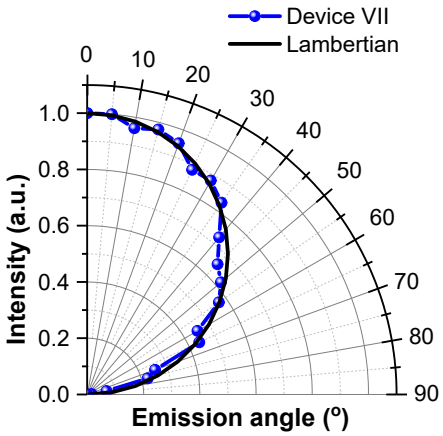

Figure S16 Normalized emission intensity angular distribution of the white OLED (device VII).

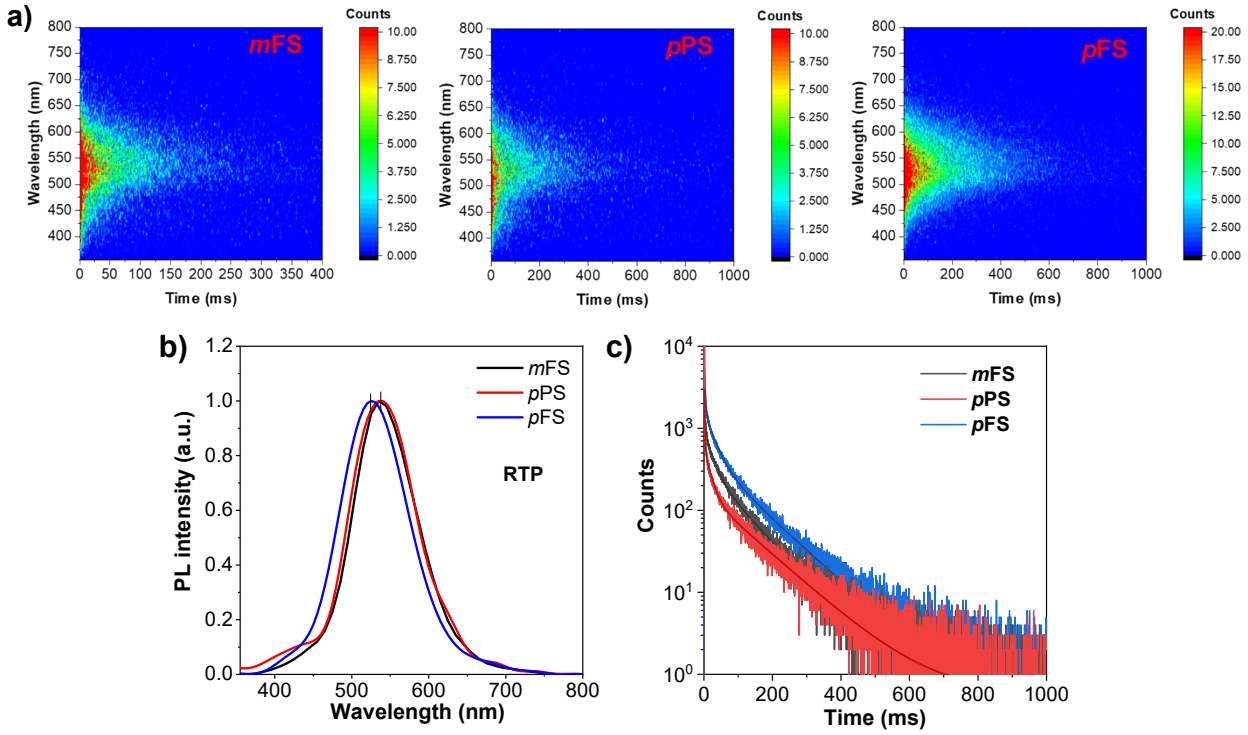

	S_1 (eV)	T_1 (eV)	ΔE_{ST} (eV)	τ (ms)
***m*FS**	2.88	2.34	0.54	65.99
***p*PS**	3.03	2.34	0.69	77.99
***p*FS**	2.98	2.36	0.62	71.87

Figure S17 a) TRES 2D contour maps (excitation at 365 nm) observing at 370-800 nm of 2 wt% doped PMMA films covered with PVA film. b) TRES slice PL spectra at 10 ms after LED turnoff of the 2 wt% doped PMMA films covered with PVA film. c) Transient PL decay spectra of RTP component.

Figure S18 Copies of HRMS MALDI–TOF/APCI–TOF mass spectra, and the ^{1}H NMR spectra (600 MHz) and ^{13}C NMR spectra (151 MHz) in $CDCl_3$ @ 25 °C.

Compound 1

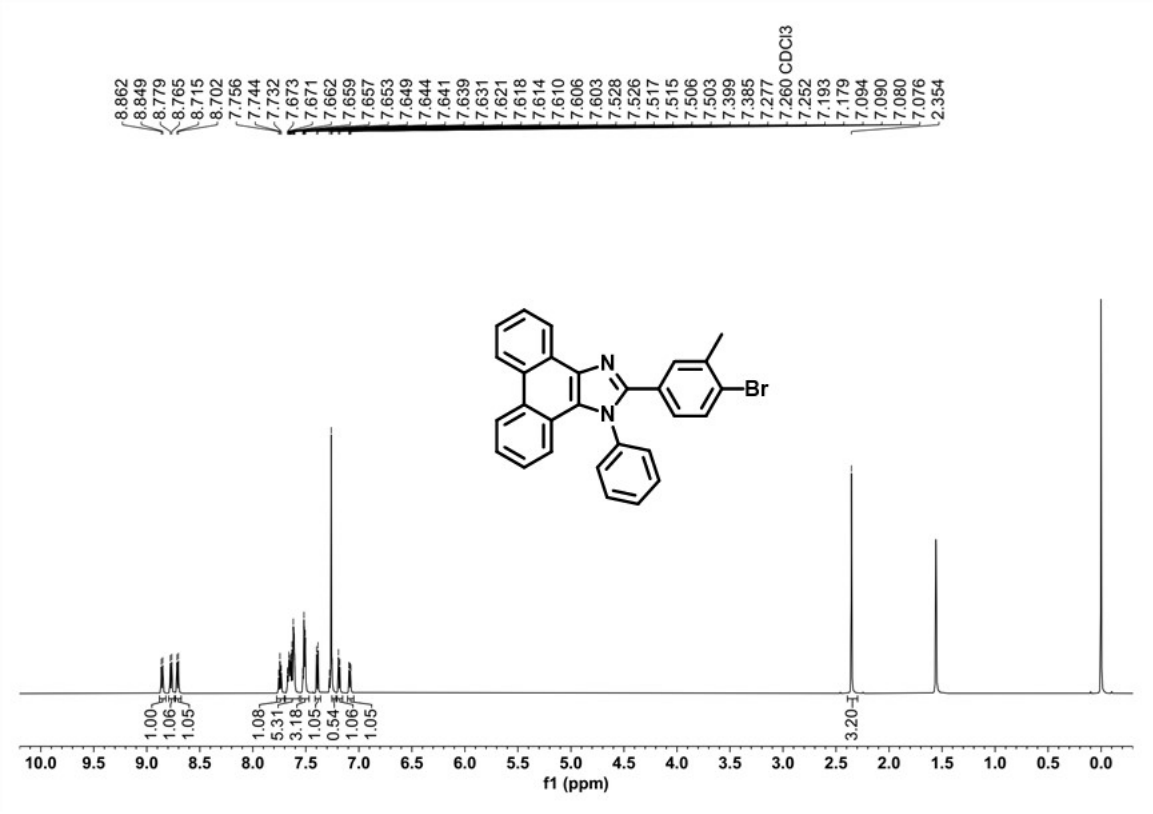

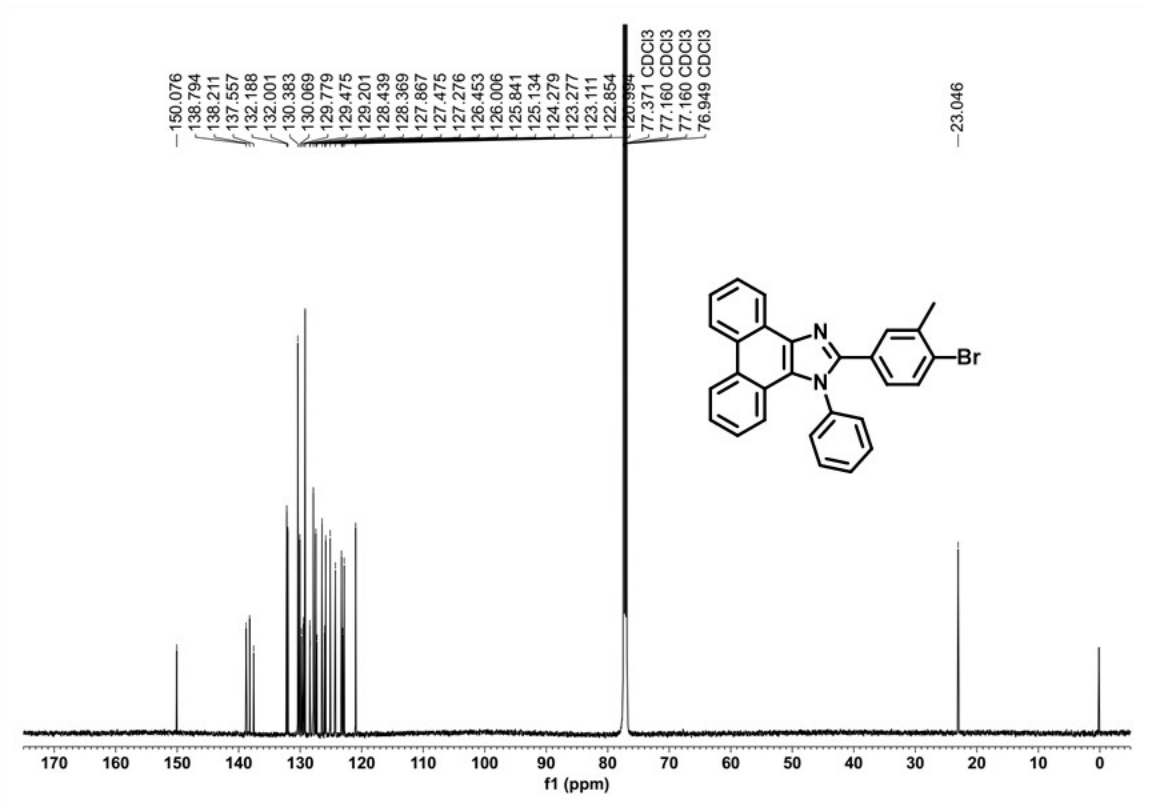

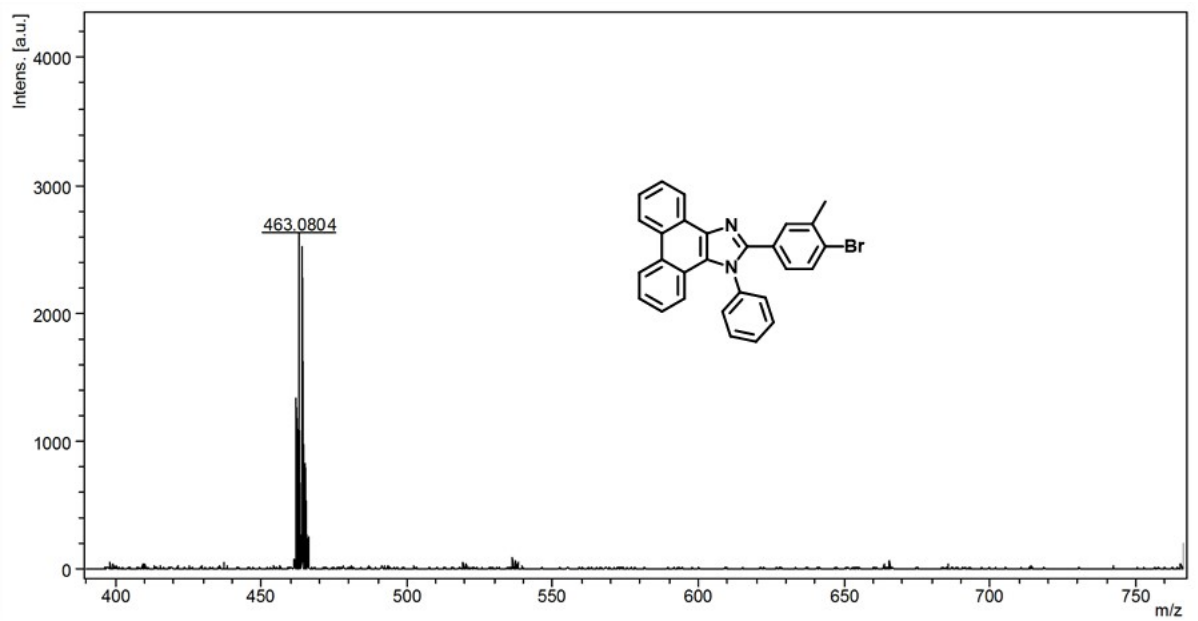
Intens. [a.u.]
4000
3000
2000
1000
0
463.0804
400
450
500
550
600
650
700
750
m/z
N
N
Br

Compound 2

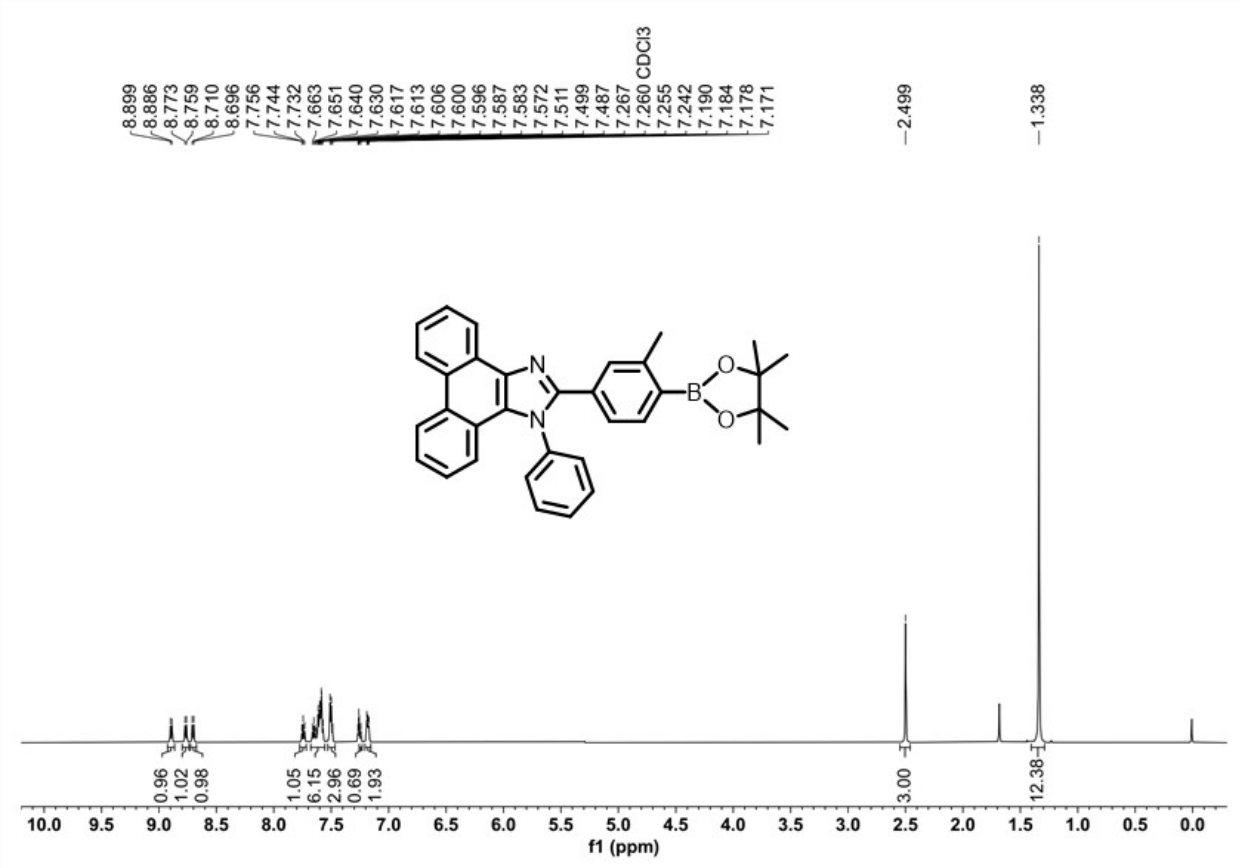
8.899
8.886
8.773
8.759
8.710
8.696
7.756
7.744
7.732
7.663
7.651
7.640
7.630
7.617
7.613
7.606
7.600
7.596
7.587
7.583
7.572
7.511
7.499
7.487
7.267
7.260 CDCl3
7.255
7.242
7.190
7.184
7.178
7.171
2.499
1.338
N
N
B
O
O
0.96
1.02
0.98
1.05
6.15
2.96
0.69
1.93
3.00
12.38
10.0
9.5
9.0
8.5
8.0
7.5
7.0
6.5
6.0
5.5
5.0
4.5
4.0
3.5
3.0
2.5
2.0
1.5
1.0
0.5
0.0
f1 (ppm)

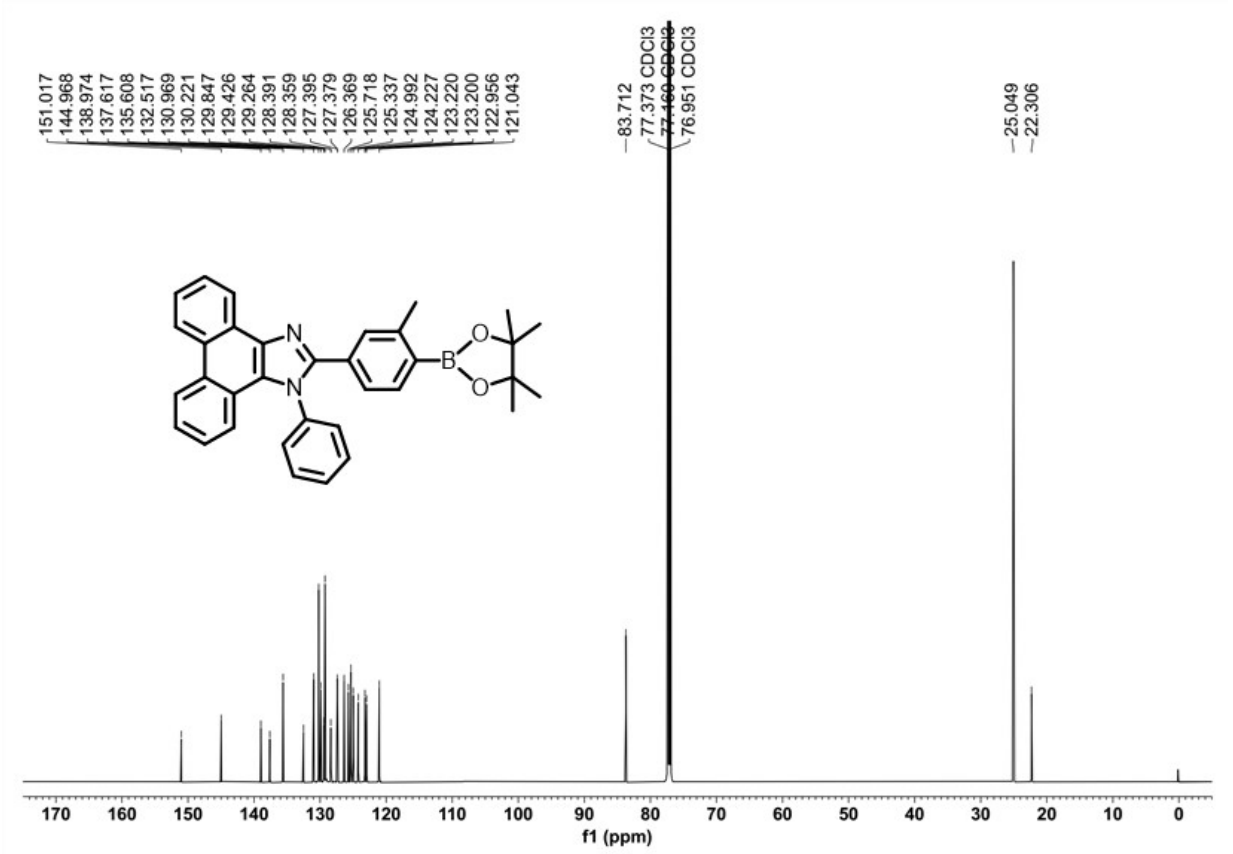
151.017
144.968
138.974
137.617
135.608
132.517
130.969
130.221
129.847
129.426
129.264
128.391
128.359
127.395
127.379
126.369
125.718
125.337
124.992
124.227
123.220
123.200
122.956
121.043
83.712
77.373 CDCl3
77.160 CDCl3
76.951 CDCl3
25.049
22.306
N
N
B
O
O
170
160
150
140
130
120
110
100
90
80
70
60
50
40
30
20
10
0
f1 (ppm)

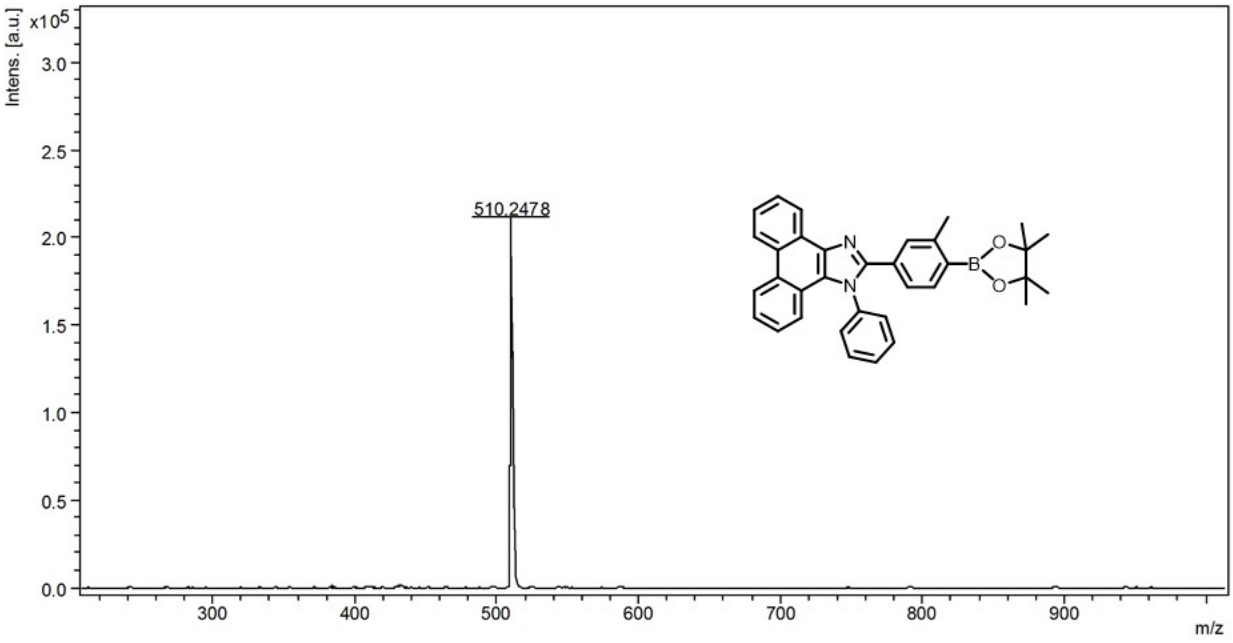
Intens. [a.u.]
x10^5
3.0
2.5
2.0
1.5
1.0
0.5
0.0
510.2478
N
N
B
O
O
300
400
500
600
700
800
900
m/z

Compound 3

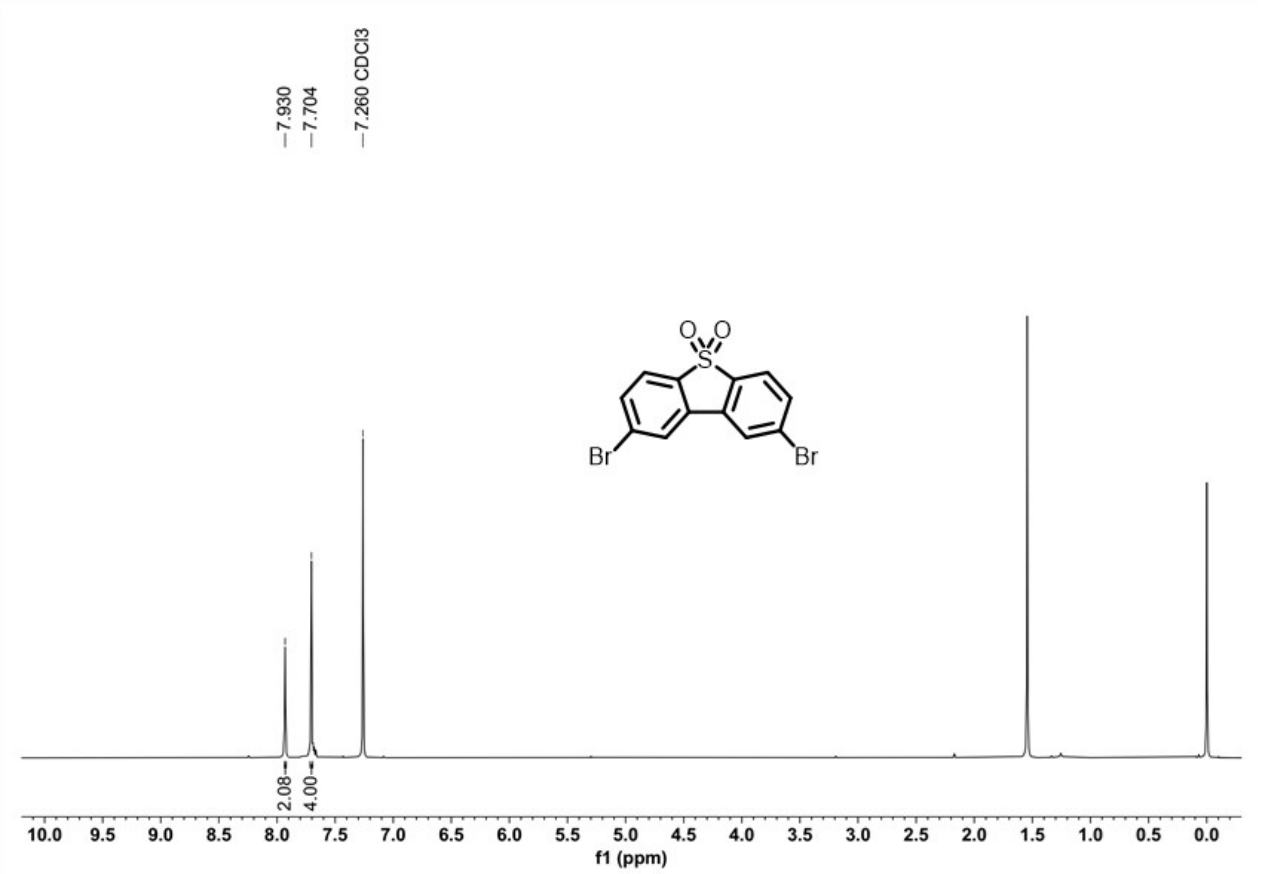
7.930
7.704
7.260 CDCl3
O
O
S
Br
Br
2.08
4.00
10.0 9.5 9.0 8.5 8.0 7.5 7.0 6.5 6.0 5.5 5.0 4.5 4.0 3.5 3.0 2.5 2.0 1.5 1.0 0.5 0.0
f1 (ppm)

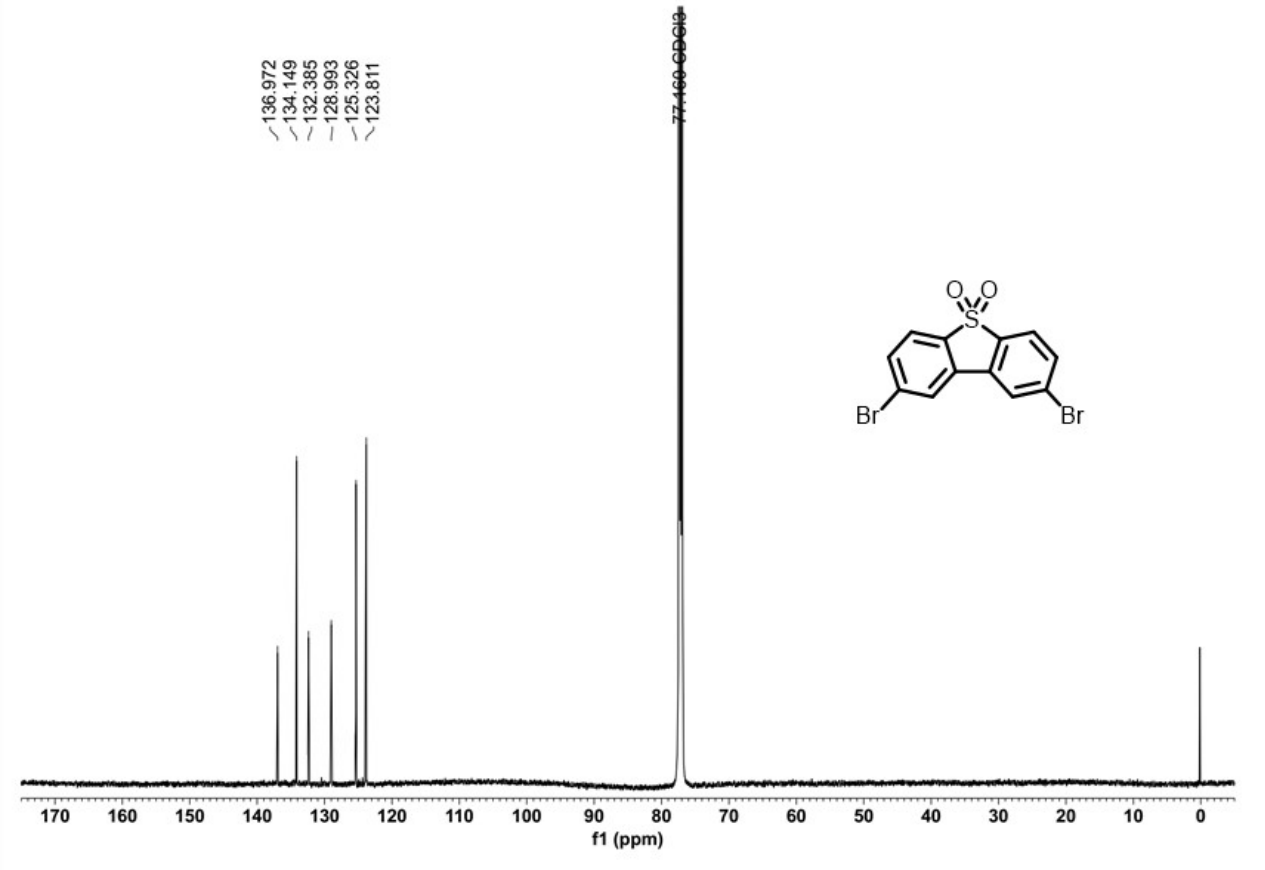
136.972
134.149
132.385
128.993
125.326
123.811
77.160 CDCl3
O
O
S
Br
Br
170 160 150 140 130 120 110 100 90 80 70 60 50 40 30 20 10 0
f1 (ppm)

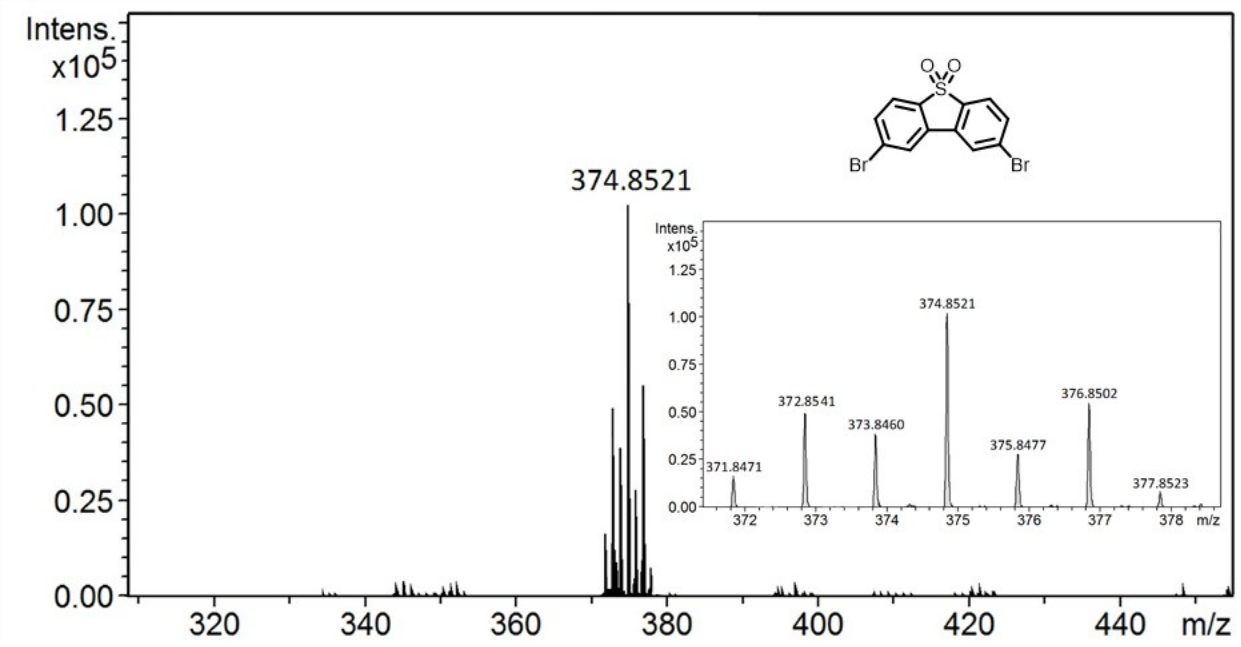
Intens.
x10^5
1.25
1.00
0.75
0.50
0.25
0.00
374.8521
Br
Br
320
340
360
380
400
420
440
m/z
372.8541
373.8460
375.8477
376.8502
371.8471
377.8523
372
373
374
375
376
377
378

Compound 4

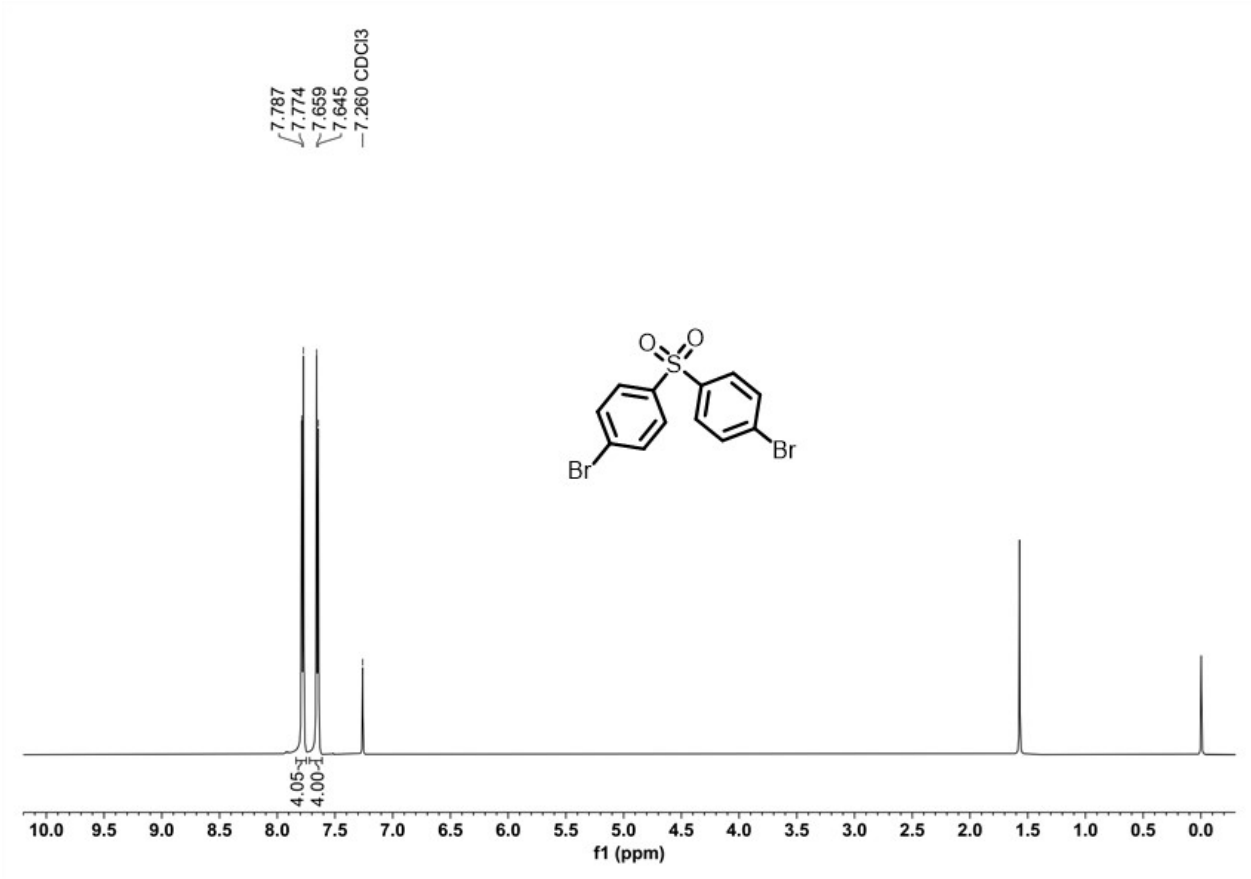
7.787
7.774
7.659
7.645
7.260 CDCl3
Br
Br
4.05
4.00
10.0
9.5
9.0
8.5
8.0
7.5
7.0
6.5
6.0
5.5
5.0
4.5
4.0
3.5
3.0
2.5
2.0
1.5
1.0
0.5
0.0
f1 (ppm)

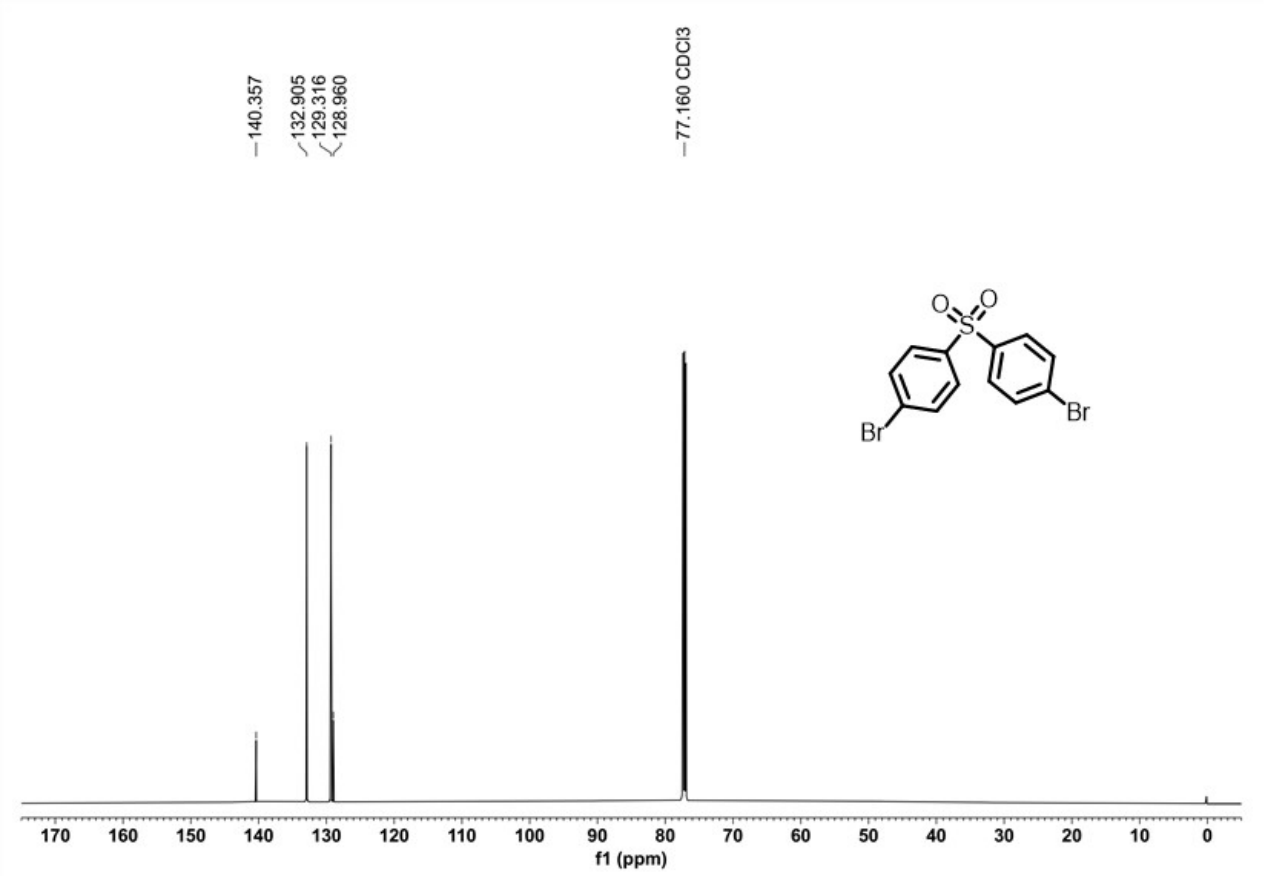
140.357
132.905
129.316
128.960
77.160 CDCl3
O
S
O
Br
Br
170 160 150 140 130 120 110 100 90 80 70 60 50 40 30 20 10 0
f1 (ppm)

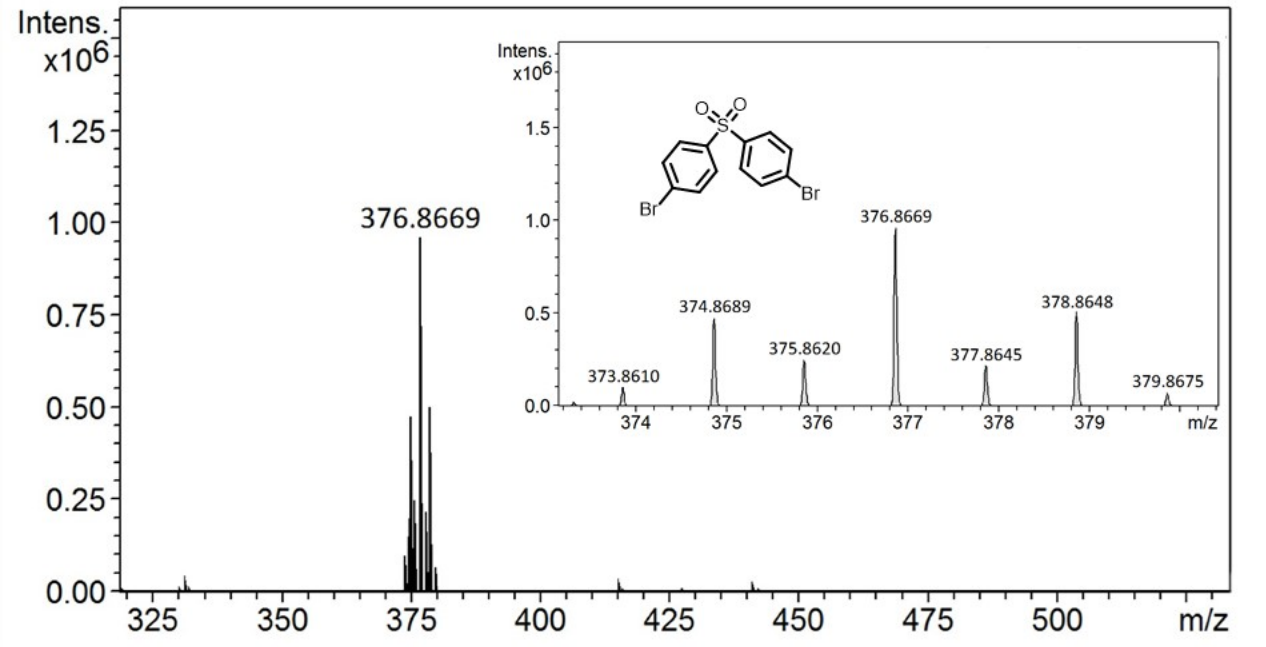
Intens.
x10^6
1.25
1.00
0.75
0.50
0.25
0.00
376.8669
325 350 375 400 425 450 475 500 m/z
Intens.
x10^6
1.5
1.0
0.5
0.0
O
S
O
Br
Br
376.8669
374.8689
375.8620
378.8648
377.8645
373.8610
379.8675
374 375 376 377 378 379 m/z

Compound *m*FS

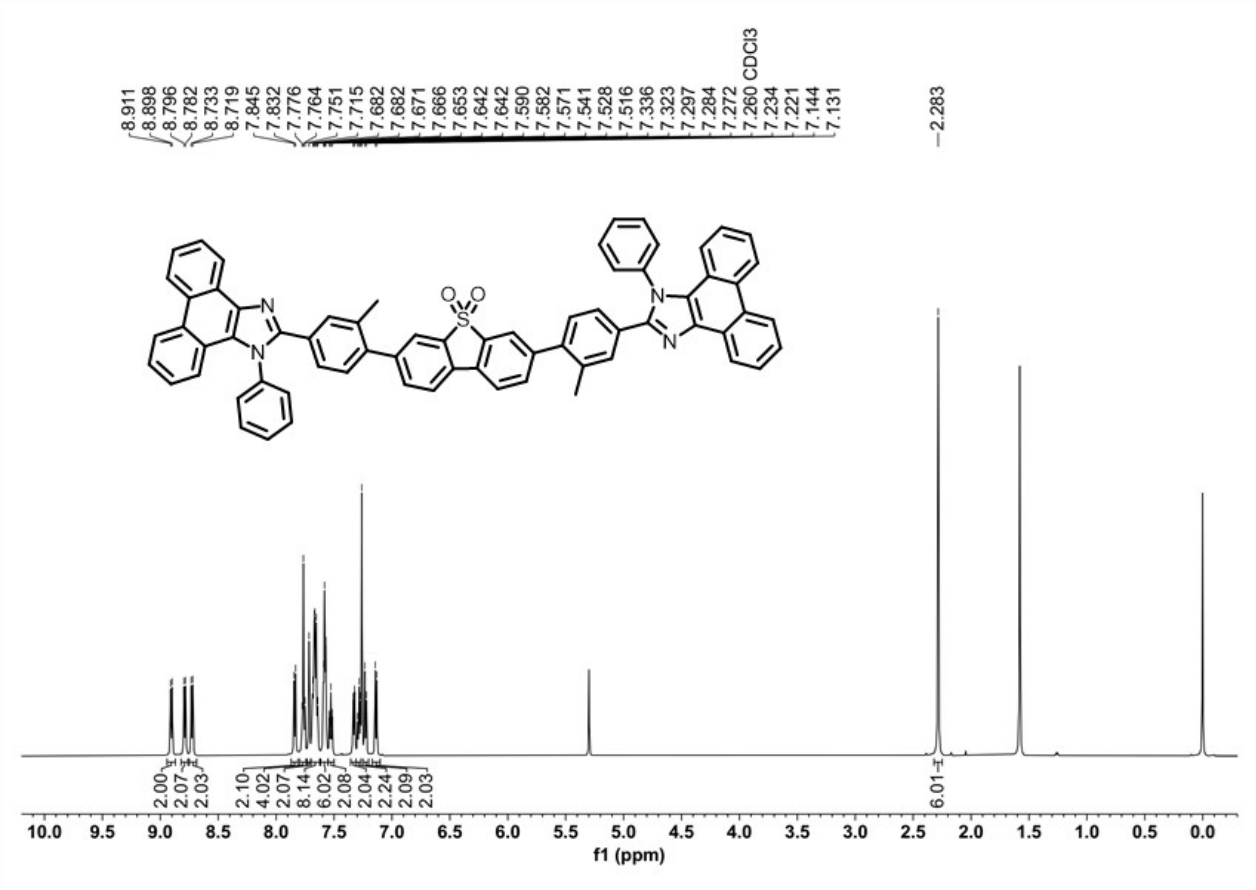

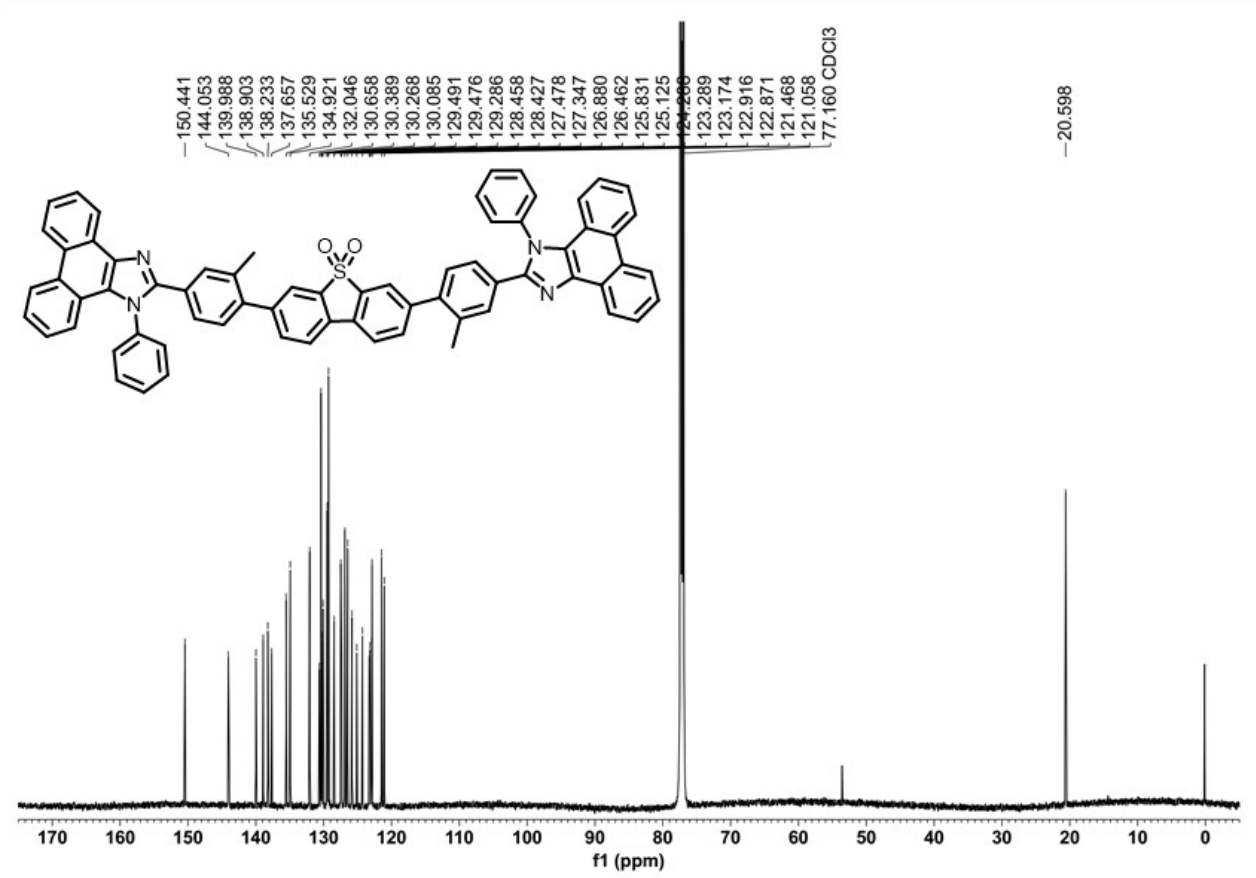

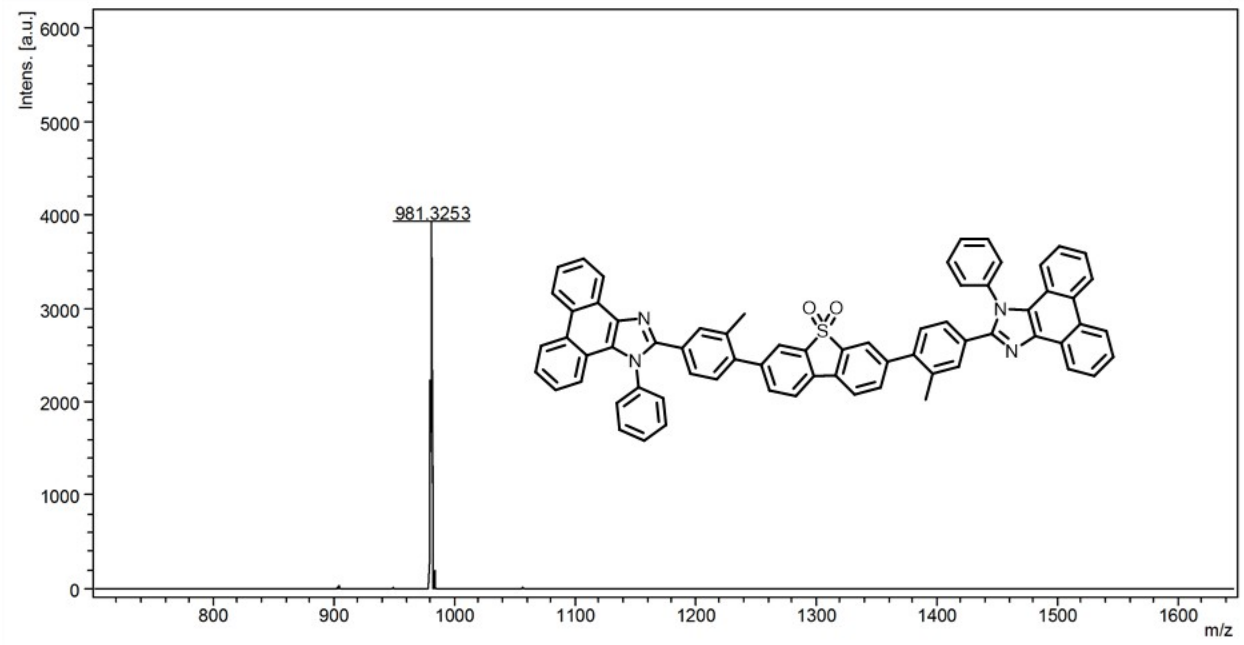

Compound *p*FS

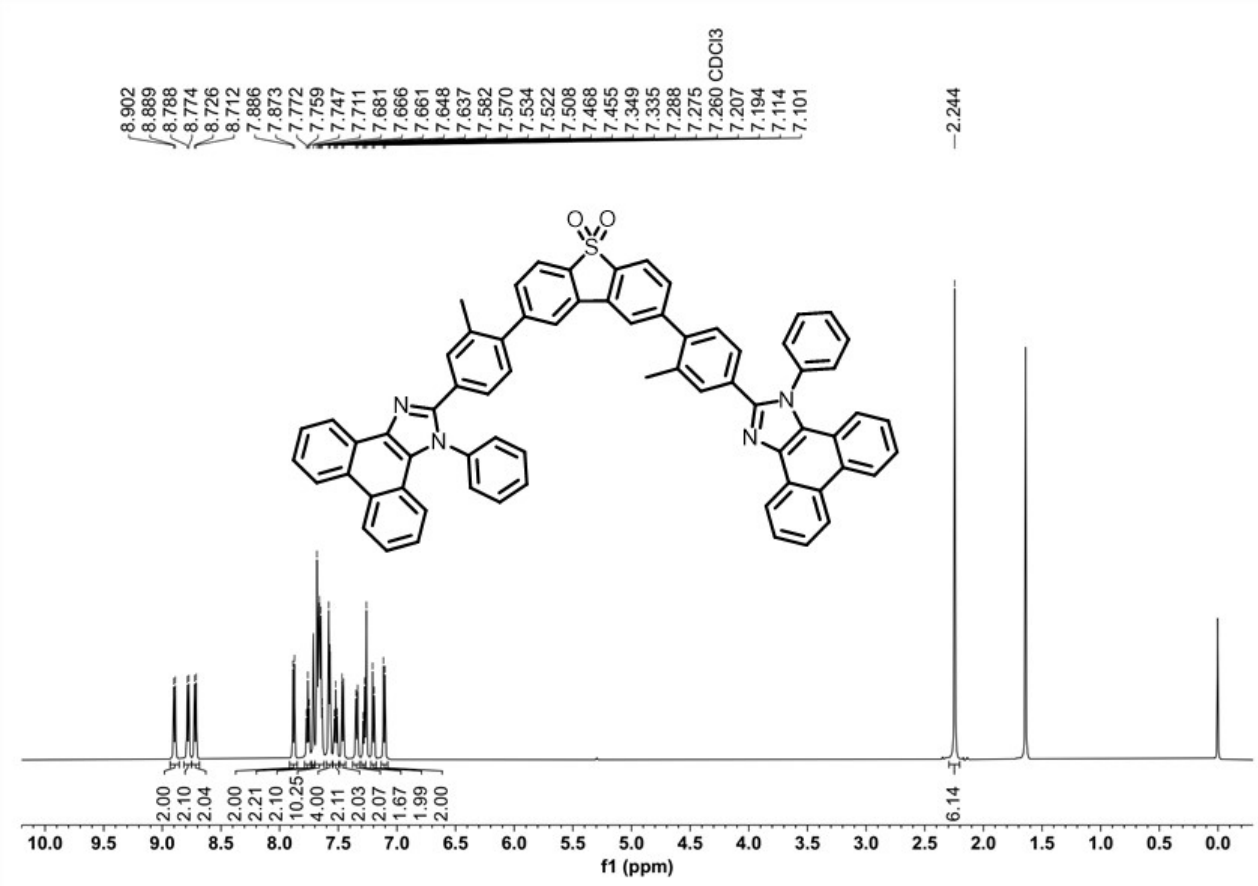

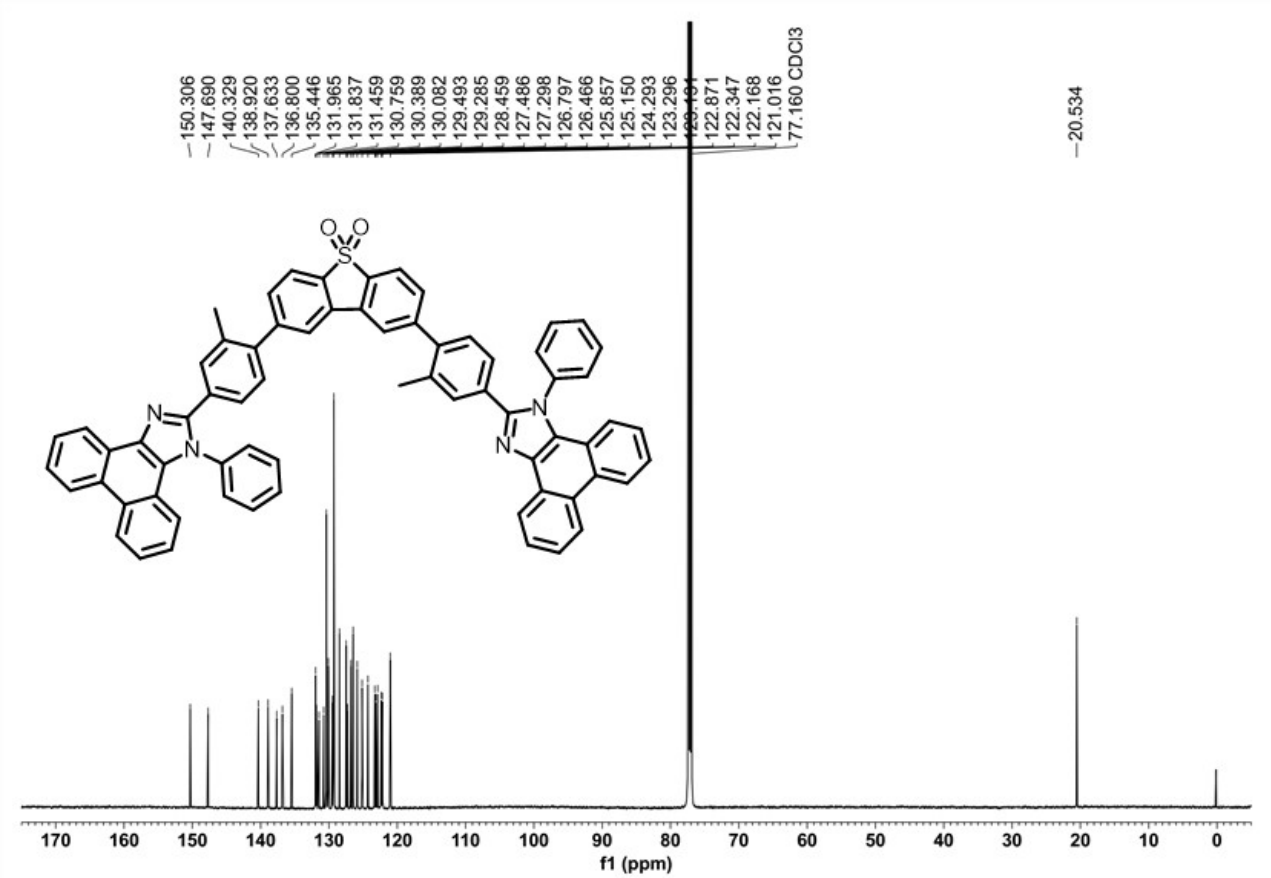
150.306
147.690
140.329
138.920
137.633
136.800
135.446
131.965
131.837
131.459
130.759
130.389
130.082
129.493
129.285
128.459
127.486
127.298
126.797
126.466
125.857
125.150
124.293
123.296
122.871
122.347
122.168
121.016
77.160 CDCl3
20.534
f1 (ppm)

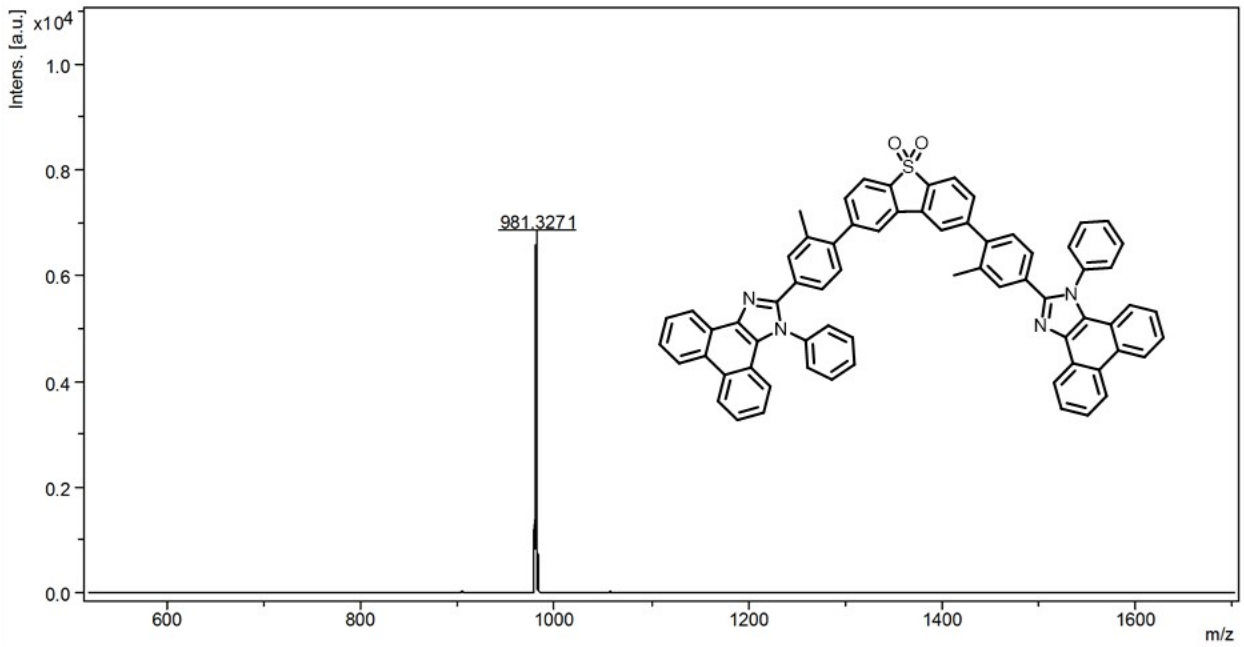
Intens. [a.u.]
x10^4
981.3271
m/z

Compound *m*PS

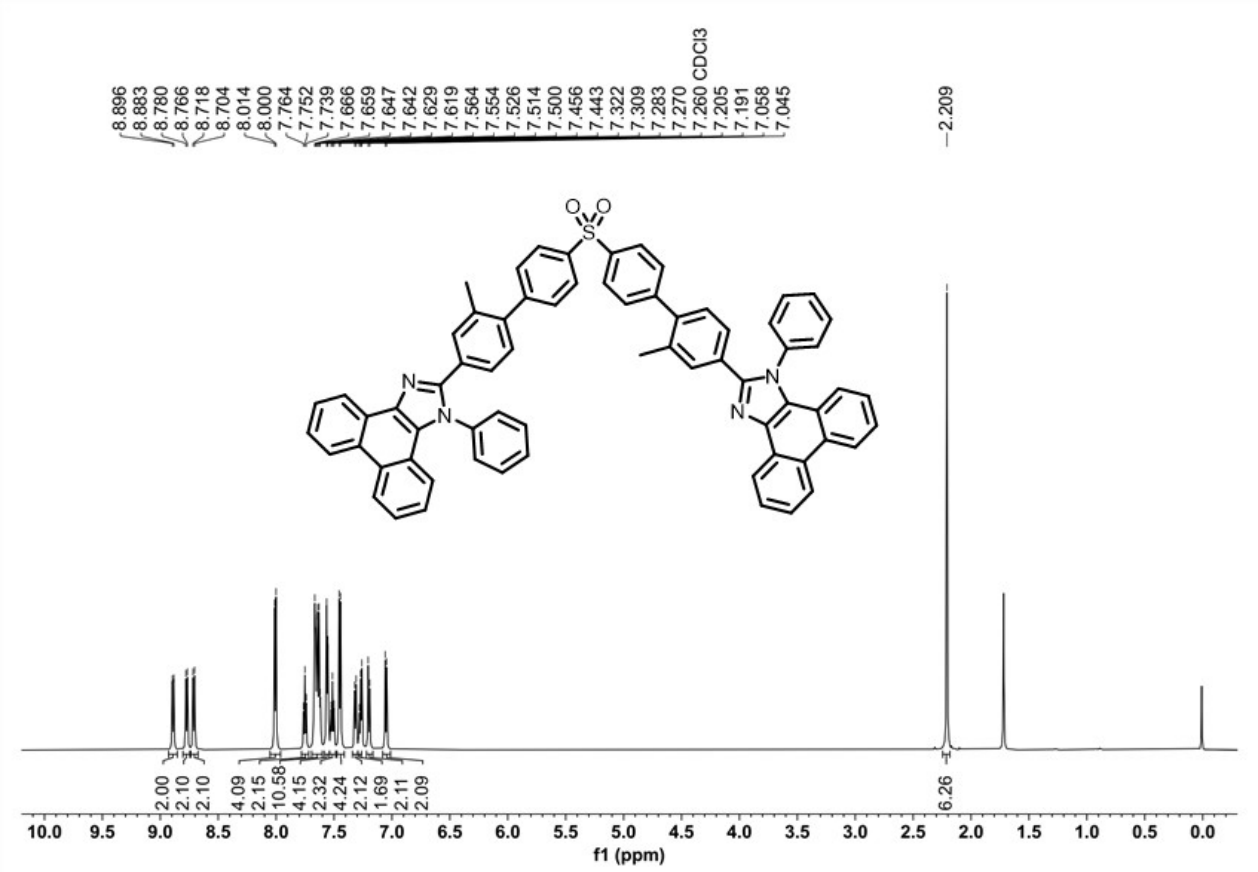

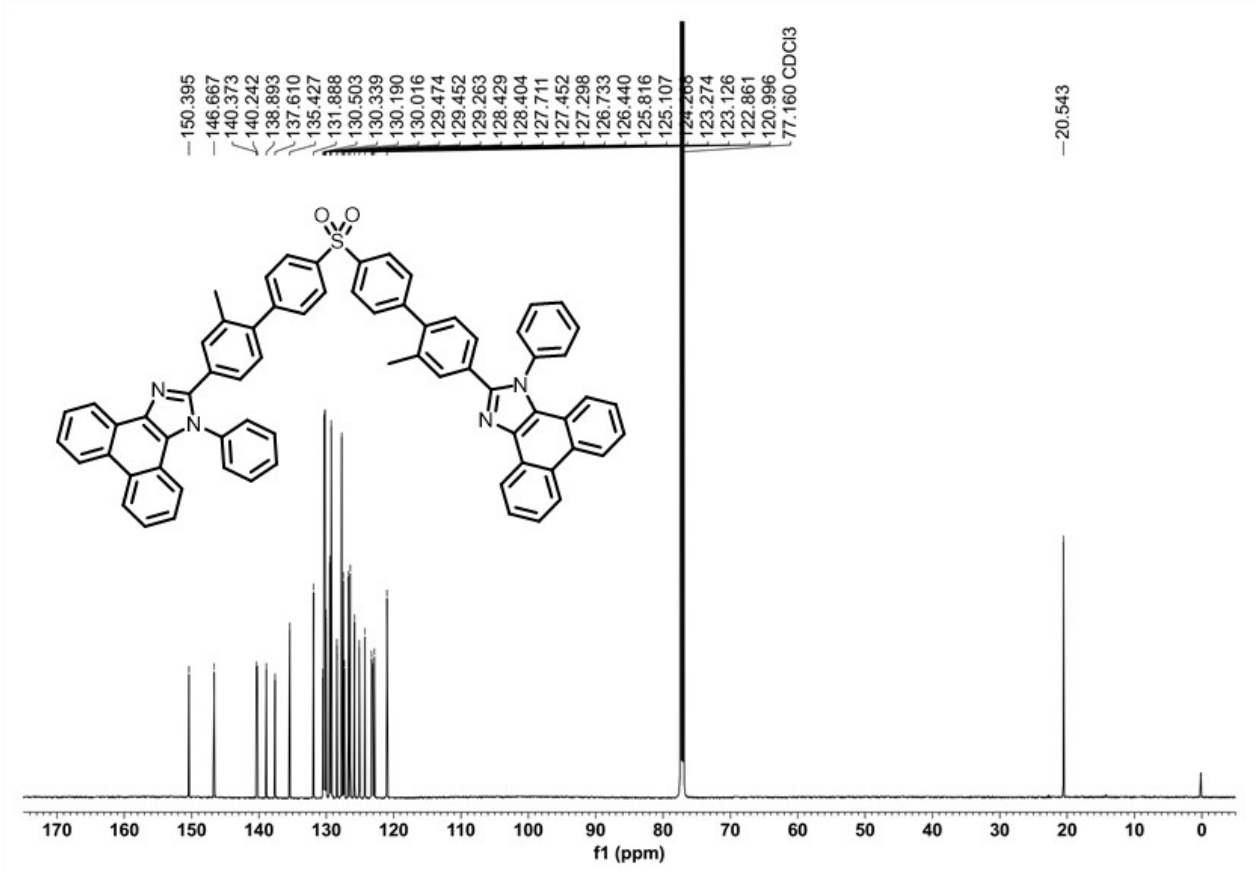

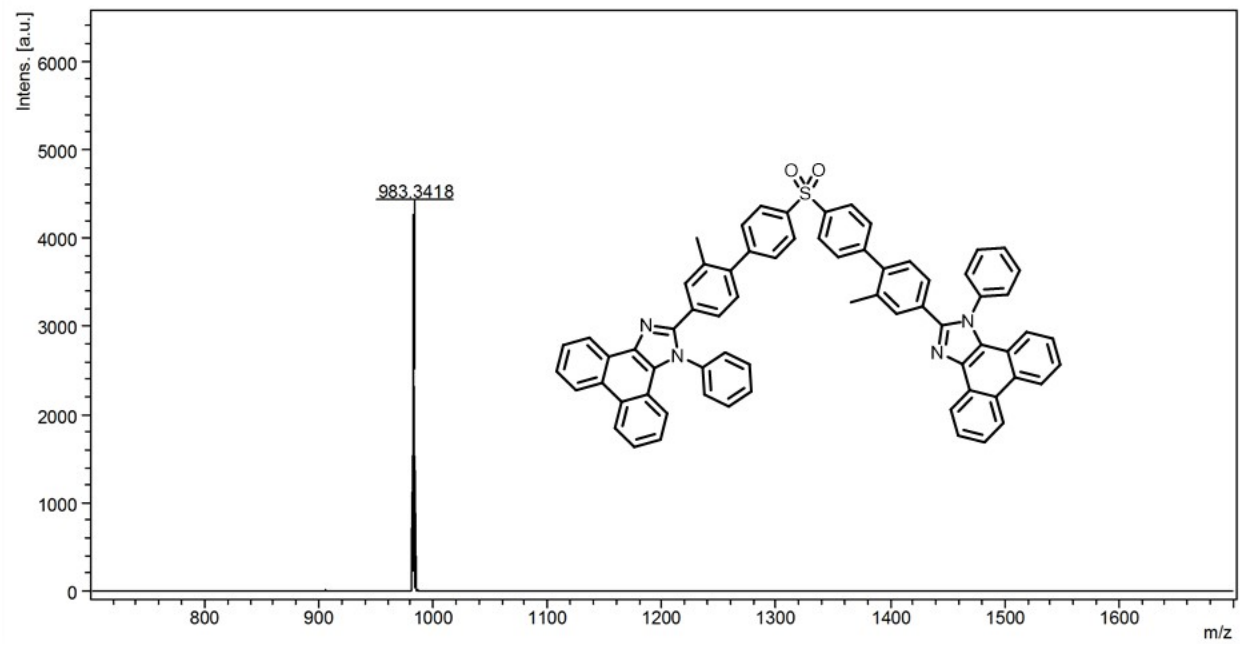

Figure S31: Molecular structures of **mFS**, **pFS**, **pPS** and relevant structures.

Table S6: The EL performances of both nondoped and doped devices based on **mFS**, **pFS**, and **pPS**, compared to that of the related molecular structures.

EMC	Device type	EQE_{max}(%)	λ_{EL}(nnm)	CIExy
PITO[5]	nondoped	3.88	480	(0.17,0.31)
	doped	4.67	444	(0.15,0.08)
PMSO[6]	nondoped	4.95	465	(0.16,0.21)
	doped	6.80	445	(0.15,0.08)
mFS (this work)	nondoped	4.13	486	(0.19,0.34)
	doped	7.24	443	(0.15,0.09)
pFS (this work)	nondoped	1.20	464	(0.21,0.27)
	doped	6.26	430	(0.16,0.07)
pPS (this work)	nondoped	5.55	450	(0.16,0.15)
	doped	6.50	420	(0.16,0.07)